# Effect of struts and central tower on aerodynamics and aeroacoustics of vertical axis wind turbines using mid-fidelity and high-fidelity methods

AIAA SciTech Forum
8-12 January 2024, Orlando, FL
AIAA SCITECH 2024 Forum

10.2514/6.2024-1485

# Effect of struts and central tower on aerodynamics and aeroacoustics of vertical axis wind turbines using mid-fidelity and high-fidelity methods

Shubham Shubham* †
*Nottingham Trent University, Nottingham, NG1 4FQ, United Kingdom*
*Cranfield University, Bedford, MK43 0AL, United Kingdom*

Francesco Avallone‡
*Politecnico di Torino, Torino, 10129, Italy*

Livia Brandetti§
*Delft University of Technology, Delft, 2629 HS, Netherlands*

Nigel Wright¶
*University of Birmingham, Birmingham, B15 2TT, United Kingdom*

Anton Ianakiev‖
*Nottingham Trent University, Nottingham, NG1 4FQ, United Kingdom*



**This study investigates the impact of struts and a central tower on the aerodynamics and aeroacoustics of Darrieus Vertical Axis Wind Turbines (VAWTs) at chord-based Reynolds numbers of $8.12 \times 10^4$. A 2-bladed H-Darrieus VAWT is used, featuring a 1.5m diameter, a solidity of 0.1 and a blade cross-section of symmetrical NACA 0021. The turbine design is kept simple and straight-bladed which is essential for isolating and analyzing the specific effects of struts and a tower. The high-fidelity Lattice Boltzmann Method (LBM) in PowerFLOW 6-2020 and the mid-fidelity Lifting Line Free Vortex Wake (LLFVW) method in QBlade 2.0 are employed, with the mid-fidelity method providing a faster analytical tool for insights into the turbine performance. Firstly, both the LLFVW (mid-fidelity) and LBM (high-fidelity) methods effectively capture the general trends observed in VAWT power performance. However, the former predicts mean thrust values that are approximately 10% higher, and mean torque values that are approximately 19% higher, in comparison to the latter. Subsequently, the former predicts lower streamwise wake velocities relative to those predicted by the latter. These differences increase in configurations that include struts and a tower (to 30% - 31%). Secondly, the presence of struts and a tower leads to a reduction in both mean power (by 15% to 55%) and thrust (by 3% to 3.6%), with a further small decrease observed when doubling the tower diameter (power and thrust both by 0.5% to 3%). The struts predominantly affect the spanwise distribution of blade loading, while the tower impacts the azimuthal variation of blade loading. Additionally, the addition of struts and a tower reduces low-frequency noise (50-200 Hz) while increasing high-frequency noise (> 300 Hz). The observed decrease in mean blade loading results in reduced low-frequency noise, while the increase in high-frequency noise is ascribed to the increased intensity of BWI/BVI leading to higher unsteady loading fluctuations on blades.**

## I. Nomenclature

*PhD researcher, Sustainable Energy Systems, Department of Civil Engineering, shubham.shubham@ntu.ac.uk, AIAA member 1345559
†Post-Doctoral Research Fellow, School of Aerospace, Transport and Manufacturing, shubham.shubham@cranfield.ac.uk
‡Professor, Department of Mechanical and Aerospace Engineering, francesco.avallone@polito.it
§PhD candidate, Faculty of Aerospace Engineering, L.Brandetti@tudelft.nl
¶Professor of Water and Environmental Engineering, Department of Civil Engineering, n.wright.4@bham.ac.uk
‖Professor, Sustainable Energy Systems, Department of Civil Engineering, anton.ianakiev@ntu.ac.uk

$c$ = blade chord, m
$C_T$ = thrust coefficient
$C_Q$ = torque coefficient
$C_P$ = power coefficient
$D$ = VAWT diameter, m
$f$ = frequency, Hz
$L$ = blade length, m
$Q$ = VAWT torque, Nm
$R$ = VAWT radius, m
$Re_c$ = chord-based Reynolds number
$T$ = VAWT thrust, N
$u$ = uncertainty
$V_\infty$ = freestream velocity, m/s
$\omega$ = VAWT rotational speed, rad/s
$\rho$ = air density, kg/m$^3$



## II. Introduction

There is an increasing focus on sustainable development goals in urban areas, which contribute significantly to a nation's carbon emissions. By adopting urban wind turbines as a sustainable energy generation solution, cities can make strides towards achieving carbon neutrality. According to a report by Wind Europe [1], the member states of the European Union (EU-27) are advised to install 30 GW of wind energy annually to successfully achieve their renewable energy objectives for 2030. However, there is a projected shortfall of 10 GW per year from 2023-2027 in meeting these targets. In this context, urban wind turbines have the potential to serve as a viable solution for bridging this gap in meeting the heightened demand.

The turbulent flow conditions prevalent in urban areas [2] have prompted the adoption of vertical axis wind turbines (VAWTs) as a more suitable option compared to horizontal axis wind turbines (HAWTs) [3]. VAWTs offer several advantages, including lower cut-in speeds, reduced noise levels, omnidirectionality (suitable for urban areas where wind directions change frequently), and ease of maintenance [4]. As a result, the aerodynamics and aeroacoustics of vertical axis wind turbines operating at low Reynolds numbers have gained significant attention in the past decade [2–5]. A common VAWT design [5, 6] is the straight-bladed Darrieus H-rotor [7], having airfoil-shaped blades that rotate vertically around an axis, primarily generating torque through lift produced by the blades [8, 9]. VAWTs offer a wide range of design possibilities [10], with the presence of a central tower and supporting struts being a critical aspect of the design that significantly influences the aerodynamic and aeroacoustic characteristics. Various numerical and experimental studies have been conducted to investigate the impact of the central tower and supporting struts on the aerodynamic performance of VAWTs, which are discussed below.

Howell et al. [11] conducted wind tunnel experiments for 2- and 3-bladed Darrieus VAWTs and compared the results with 2D and 3D CFD simulations using the RANS method. Significant differences were observed between the power coefficients ($C_P$) obtained by 2D and 3D simulations, where the former predicted values were 2-8 times higher than the latter. This was attributed to the presence of blade tip vortices, flow divergence and additional struts and a central tower. Similar order of magnitude differences in 2D and 3D CFD results were also obtained by various authors [12–15]. Elkhoury et al. [16] carried out LES simulations along with wind tunnel experiments for a VAWT. The author mentioned that the effect of connecting rods in a VAWT can only be neglected at low TSRs since their effect on $C_P$ values increases with TSR. Miao et al. [17] conducted CFD simulations using the Improved Detached Eddy Simulation (IDDES) method using various strut profiles and found out that the profile and induced drag of struts reduce the VAWT efficiency. The author also reported a linear increase in strut drag with an increase in profile thickness and a reduction in strut drag with an increase in chord length. Siddiqui et al. [18] also conducted CFD simulations using the RANS method and reported a decrease in VAWT efficiency and power production, additional profile drag and generation of strong 3D vortices due to the addition of struts and a central hub.

De Marco et al. [19] conducted RANS simulations and showed that a balance is required in the number of VAWT strut elements to achieve optimal aerodynamic performance, the finding of which is very similar to the effect of the number of blades [5, 20]. Aihara et al. [21] employed the 3D RANS method to investigate the impact of struts and towers on the distribution of blade force and VAWT rotor performance. The results indicate that while the presence of struts significantly affects the blade force distribution and power coefficient, the tower effect does not produce

remarkable differences. To investigate different strut profiles, Bachant et al. [22] conducted a comparative study of the drag characteristics of a NACA 0021 airfoil and a cylinder strut. The high drag exhibited by the cylinder strut severely impeded power generation, whereas the NACA airfoil strut experienced comparatively lower power losses and has lower profile drag. Other authors have also suggested airfoil-shaped struts for better aerodynamic performance [23, 24].

Struts can also be modelled with mid-fidelity methods, which are capable of a faster analysis as compared to the aforementioned CFD methods. This includes the 3D nonlinear lifting line method [25] in which the effect of struts can be included as lifting bodies. Mendoza et al. [26] performed simulations using the 3D actuator line method and showed that the VAWT wake structure was not significantly affected by either removing struts or the central tower and therefore had a limited impact on overall performance.

An essential factor in increasing VAWT public acceptance is the reduction of noise generation [27, 28], which can be affected by the presence of struts and a central tower. Although only limited studies have been conducted on noise sources in VAWTs, in contrast to extensive investigations on large-scale Horizontal Axis Wind Turbines (HAWTs). The knowledge gained from the noise studies of HAWTs cannot be applied directly to develop low-noise small-scale VAWTs, mainly because of the differences in aerodynamic phenomena at Reynolds numbers ($Re$) ranging from $1 \times 10^4$ to $1 \times 10^5$ for the latter, and differences in fluid dynamic interactions due to the axis of rotation of VAWTs being perpendicular to that of HAWTs. Several studies have reported that VAWTs produce lower noise than HAWTs of similar size and power, which makes them suitable for applications in urban areas [29–31].

Despite the available literature, there is a lack of systematic in-depth investigations into unsteady blade loads and downstream turbulent near-wake of VAWTs using full 3D high-fidelity numerical simulations to understand the effect of struts and tower. Furthermore, the capability of mid-fidelity analytical aerodynamic methods to capture the effects of struts and a central tower on VAWT force and flow field is not well understood. Therefore, the present study performs simulations using a multi-fidelity simulation framework, which aims to combine the accuracy of the high-fidelity method and the speed of numerical simulations of the mid-fidelity method. This is achieved by conducting high-fidelity aerodynamic simulations using the Lattice Boltzmann Method (LBM) and mid-fidelity simulations using the Lifting Line Free Vortex Wake (LLFVW) method for straight-bladed VAWTs. Furthermore, aeroacoustic post-processing is performed using the Ffowcs Williams and Hawkings (FW-H) methodology to calculate the far-field noise, to identify the impact of struts and central tower on VAWT aeroacoustic performance and noise sources.

The first objective is to compare the results obtained using the mid-fidelity and high-fidelity methods and investigate any differences observed. Secondly, the aim is to gain insights into the different fluid dynamic interactions that arise due to the presence of struts and a central tower. Finally, the effect of struts and a central tower on VAWT aeroacoustics will be understood which will be crucial in developing low-noise designs. High-fidelity simulations enable accurate resolution of flow around VAWT blades and downstream wake, while, the mid-fidelity simulation offers simplified modelling of the flow field using vortex lifting lines and aids in only a fundamental understanding of the 3D effects such as non-uniform blade loading and wake, dynamic stall, blade-vortex interaction, and wake recovery. A comparative analysis between the two methods can also determine the potential of the mid-fidelity method as a substitute for high-fidelity simulation to save significant time and computational resources.

The paper is structured as follows. Section III presents the computational methodology used in QBlade and PowerFLOW. Section IV describes the geometry and setup used. Section V presents the results obtained using both mid-fidelity LLFVW and high-fidelity LBM for all three VAWT configurations. Finally, section VI outlines the conclusions of the current study and suggests future recommendations.

## III. Computational Methodology

This section describes the computational methodologies employed in the study, focusing on two flow solvers: QBlade and PowerFLOW. These solvers are instrumental in analyzing the aerodynamic and aeroacoustic performance of Vertical Axis Wind Turbines (VAWTs) under various configurations. The methodologies are chosen for their proven accuracy and efficiency in similar low Reynolds number rotor applications, providing a comprehensive understanding of the VAWT force and flow field.

### A. Flow solver - QBlade

The lifting line method is used to compute the force and flow field because it was shown to be accurate and efficient for similar low Reynolds number rotor applications [32–34]. This method is a part of the broader category of vortex methods, characterized by a computational cost that is intermediate between low-fidelity momentum methods (such as BEMT and DMS) and high-fidelity Computational Fluid Dynamics (CFD) methods, including Navier-Stokes and

Lattice-Boltzmann approaches. In the present study, the lifting line theory coupled to a free vortex wake model is used to calculate the VAWT three-dimensional (3D) unsteady flow field past the rotor and the interaction between blade and fluid flow [35, 36]. The LLFVW algorithm is based on nonlinear lifting line formulation by Garrel [37] and is mentioned in detail by Balduzzi [36].

The fluid is modelled as incompressible, inviscid and irrotational; the blade is modelled with a single line of vortices which is located on the quarter chord points of the blade. The wake is discretised into vortex line elements (straight or curved) and these elements are shed at the blade trailing edges at every time step. They then undergo free convection past the rotor ("free wake method") in which the position of the wake end nodes is updated based on the local velocity, which is a combination of inflow velocity and induced velocity from all the wake elements in the domain. Nonlinear in the "nonlinear lifting line formulation" means the circulation calculated on the lifting line bound vortices is acquired from the nonlinear airfoil lift and drag data provided as input. Lift and drag forces are then calculated based on the local angle of attack ($\alpha$).

The vortex elements are desingularised using the van Garrel's cut-off method [38] with the vortex core size, taking into account viscous diffusion via the vortex core size that is modelled through the kinematic viscosity $\nu$, a turbulent vortex viscosity coefficient $\delta_\nu$, and a time offset parameter $S_c$ using the below equation:

$$r_c = \left( \frac{5.03 \delta_\nu \nu \left(t + S_c\right)}{1 + \varepsilon} \right)^{1/2} \tag{1}$$

The effects of unsteady aerodynamics and dynamic stall are introduced via the ATEFlap aerodynamic model [39, 40] that reconstructs lift and drag hysteresis curves from a decomposition of the lift polars. The implemented ATEFlap formulation has been further adapted to work under the complex conditions of VAWT exhibiting large fluctuations in the angle of attack when rotating at low TSR [41]. Wake reduction schemes have been implemented to lower computational requirements [39–42]. In the present study, all results with this method will henceforth be referred to with the 'LLFVW' nomenclature.

### B. Flow solver - PowerFLOW

The Lattice Boltzmann Method (LBM) is used to compute the flow field because it was shown to be accurate and efficient for similar low Reynolds number rotor applications [32, 43–46]. The commercial software 3DS Simulia PowerFLOW has been already validated for aerodynamic and aeroacoustic studies on rotors in general [47–49]. The software solves the discrete Lattice Boltzmann (LB) equation for a finite number of directions. For a detailed description of the method, the reader can refer to Succi [50] and Shan et al. [51], while to Chen and Doolen [52] for a review. The LB method determines the macroscopic flow variables starting from the mesoscopic kinetic equation, i.e. the LB equation. The discretization used for this particular application consists of 19 discrete velocities in three dimensions (D3Q19), involving a third-order truncation of the Chapman-Enskog expansion [53]. The distribution of particles is solved by means of the LB equation on a Cartesian mesh, known as a lattice. An explicit time integration and a collision model are used. For the collision term, the formulation based on a unique Galilean invariant [54] is used. The equilibrium distribution of Maxwell-Boltzmann is adopted [53].

To take into account the effect of the sub-grid unresolved scales of turbulence, a Very Large Eddy Simulation (VLES) model is implemented. Following Yakhot and Orszag [55], a two-equations $k - \epsilon$ Renormalization Group is used to compute a turbulent relaxation time that is added to the viscous relaxation time. To reduce the computational cost, a pressure-gradient-extended wall-model is used to approximate the no-slip boundary condition on solid walls [56, 57]. The model is based on the extension of the generalised law-of-the-wall model [58] to take into account the effect of pressure gradient. These equations are iteratively solved from the first cell close to the wall in order to specify the boundary conditions of the turbulence model. For this purpose, a slip algorithm [52], obtained as generalization of a bounce-back and specular reflection process, is used.

Far-field noise is computed using the Ffowcs Williams and Hawkings [59] (FW-H) acoustic analogy. In particular, the formulation 1A of Farassat and Succi [60] extended to a convective wave equation is used in this study [61]. The formulation has been implemented in the time domain using a source-time dominant algorithm [62]. Pressure fluctuations are recorded on three permeable surfaces enclosing the wind turbine and its wake. These pressure fluctuations are used as input to the FW-H solver, thereby including all noise sources inside the three surfaces. Pressure fluctuations are also captured on all solid surfaces (blade surfaces), which when input to the FW-H solver will include noise sources only on the solid surfaces. In the present study, all results with this method will henceforth be referred to with the 'LBM' nomenclature.

# IV. Geometry and Setup

## A. Wind turbine geometry

Three different geometric configurations of straight-bladed Darrieus VAWT are simulated in the current study. The geometric models for the first two configurations are shown in Figure 1. The first configuration consists of only two blades, without struts and a central tower. The second configuration consists of two blades along with four struts (connected to each blade at 24% of the length of the blade) and a central tower (designated as Tower A), which is the same geometry used by Brandetti et al. [43]. For validation, numerical findings from Brandetti et al. [43] and experimental data from LeBlanc et al. [63, 64] are employed. It is important to note that while the reference studies employ boundary layer (BL) trips at a 15% chord location, on both the pressure and suction sides of the blade, the current investigation does not use them. The experimental results are present for both with and without trip, and the latter will be used for validating the results of the current study. Finally, in the third configuration, the diameter of the central tower is increased to twice the diameter of the second configuration and the tower is named 'Tower B'. Table 1 presents the geometric values for all configurations and Table 2 presents the geometric values for the struts and central tower. The VAWT solidity is set at 0.1 and the rotor aspect ratio is 1 for all configurations.

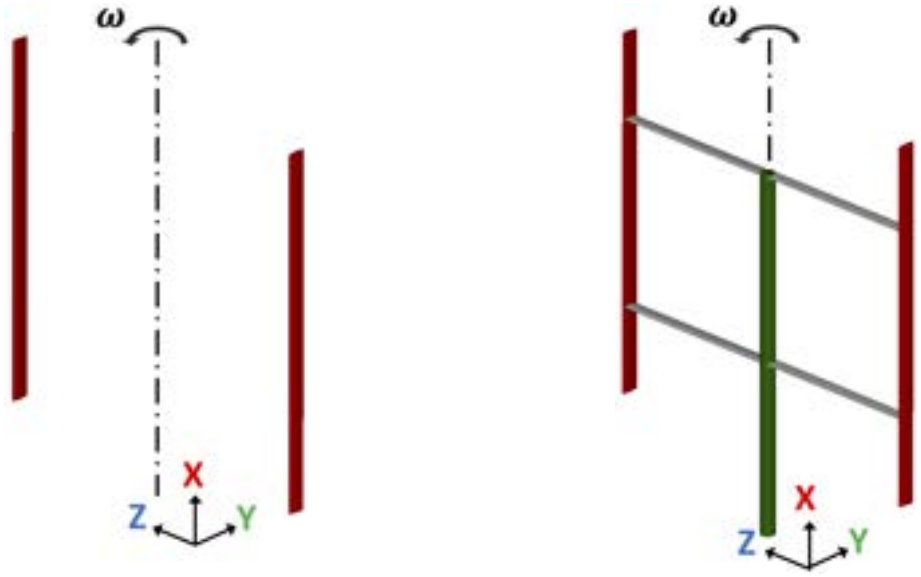


(a) First configuration - only the two blades

(b) Second configuration - two blades, with struts and central tower A

**Fig. 1 First two VAWT geometric configurations used in this chapter; for the third configuration, the diameter of the central tower, referred to as Tower B, is increased to twice that of Tower A while keeping the struts unchanged**

**Table 1 VAWT geometrical parameters for all three configurations**

| Blade length ($L$) | Rotor diameter ($D$) | Blade chord ($c$) | Blade airfoil |
|---|---|---|---|
| 1.5 m | 1.5 m | 0.075 m | NACA 0021 |

The current study involves high-fidelity LBM to simulate all the VAWT configurations. Each configuration is also simulated using the mid-fidelity LLFVW method. Ensuring the accuracy and quality of airfoil polar data is crucial for the accuracy of results in mid-fidelity aerodynamic simulations. To ensure this, XFoil [65] is used to obtain the lift and drag polars for the NACA 0021 airfoil (shown in Figure 2 (a)) for Reynolds numbers ranging between $5 \times 10^4$ to $1 \times 10^6$. This process employs an *NCrit* value of nine and forced transition at the leading edge of both the pressure and suction side. The airfoil static polar data is extrapolated to 360° angle of attack (AoA) using the Montgomerie method [66] to

**Table 2 Geometrical parameters for the struts and central tower, labelled as Tower A, in the second configuration; for the third configuration, the diameter of the central tower, referred to as Tower B, is increased to twice that of Tower A while keeping the struts unchanged**

| Strut length ($L_s$) | Strut chord ($c_s$) | Strut airfoil | Strut location | Tower diameter ($D_t$) | Tower length ($L_t$) |
|---|---|---|---|---|---|
| 0.75 m | 0.06 m | NACA 0018 | 0.36 m from blade tips | 0.06 m | 1.5 m |

ensure a smooth extrapolation in the post-stall regime. The same method for 360° polar extrapolation for a VAWT is also used by Balduzzi et al. [36].

### B. Numerical setup

For the high-fidelity LBM setup, a cubic simulation volume of $100D$ per side is employed, with the Darrieus geometry positioned at the centre. Boundary conditions are described in Figure 2 (b). The velocity inlet corresponds to the freestream velocity $V_\infty$ along the Y-axis, while an ambient pressure of 101.325 kPa characterizes the pressure outlet. The blade surface has a no-slip boundary condition.

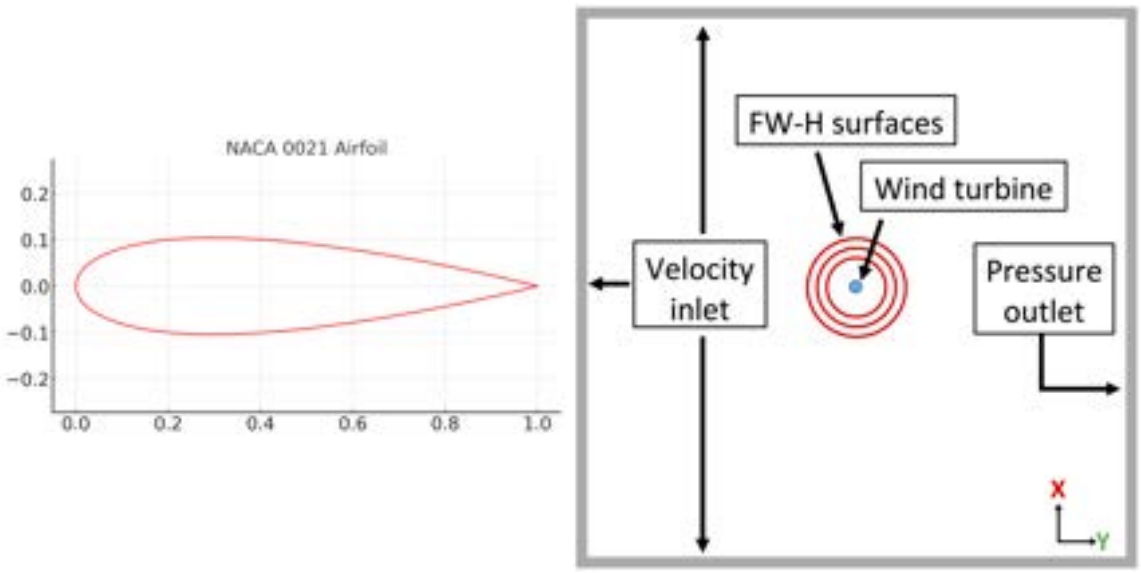


(a) (b)

**Fig. 2 Numerical setup (a) NACA 0021 airfoil (b) Schematic representation of the simulation domain for the high-fidelity simulation**

PowerFLOW constructs a Cartesian volume grid around the solid components in the domain, starting with the smallest hexahedral cell (voxel) size and a designated number of variable resolution (VR) levels. For computational efficiency, this study employs 17 VR levels, with higher resolutions in proximity to the blade and strut surfaces and coarser resolutions situated further away from them. This approach helps in allocating the computational resources to regions of significant interest and where high-flow gradients are expected. VR levels span from fine to coarse, with a voxel size factor of 2 between successive VRs, which creates distinct VR regions. The software seamlessly integrates the Cartesian mesh with solid components, generating a set of polygons, termed surfels, which accurately depict the solid body surface.

Figure 2 (b) presents three red spherical surfaces enclosing the rotor flow field, which function as FW-H permeable surfaces to eliminate hydrodynamic fluctuations arising from the VAWT wake vortices. The averaging of pressure data obtained from all the permeable surfaces assists in reducing those spurious noise sources. The blade surfaces of the VAWT are identified as FW-H solid surfaces. Although the use of the FW-H permeable formulation is a possible

alternative, it has not been utilised in this study since it is difficult to eliminate spurious noise sources from FW-H permeable data using only three spherical surfaces in the context of a VAWT. In future studies, a separate investigation will examine the implementation of the FW-H permeable formulation for VAWT aeroacoustics more efficiently. To ensure accurate acoustic wave capture, a criterion of a minimum of 15 points per wavelength is selected, and pressure data are sampled at 8000 Hz for 12 complete rotor rotations. Subsequently, noise spectra are calculated using a Hanning window with 50% overlap and a frequency resolution (Δf) of 15 Hz.

For the mid-fidelity LLFVW simulation, Table 3 outlines the values of the simulation parameters utilised which are adopted from previous studies [32, 36].

**Table 3 Simulation parameters used for the LLFVW method**

| | **LLFVW** |
|---|---|
| Density | 1.225 kg/m$^3$ |
| Kinematic viscosity | 1.65 e-5 m$^2$/s |
| Blade discretization | 21 (cosine) |
| Azimuthal discretization | 3 deg |
| Full wake length | 12 |
| Vortex time offset | 1 e-4 sec |
| Turbulent vortex viscosity | 20 |



### C. Flow conditions and grid settings

In this study, the VAWT operational parameters are listed in Table 4. The system's operational condition is quantified using the tip speed ratio (TSR), defined as the ratio of the blade rotational speed to the freestream velocity, represented as $\omega R/V_\infty$. Here, $\omega$, $R$, and $V_\infty$ denote the rotational speed, rotor radius, and freestream velocity, respectively. The freestream velocity remains consistent at 4 m/s, aligning with the reference study by Brandetti et al. [43], while variations to $\omega$ modify the TSR. The chord-based Reynolds number ($Re_c$) is calculated to be $8.12 \times 10^4$, based on the mean velocity the VAWT blade encounters in a single rotation.

**Table 4 VAWT operational setting for the high-fidelity method (LBM); mid-fidelity (LLFVW) is used for TSR 1 to 7**

| **Parameter** | **Value** |
|---|---|
| Tip speed ratio (TSR) | 4 |
| Rotational speed | 203.718 RPM |
| Freestream velocity $V_\infty$ | 4 m/s |
| Chord-based Reynolds number ($Re_c$) | $8.12 \times 10^4$ |

The freestream turbulence intensity ($I_t$) and turbulence length scale ($L_t$) are designated as 0.1% and 1 mm, respectively. A previous study by Casalino et al. [48] suggests that these parameters likely exert negligible influence on the evolution of the unsteady flow field. All operational conditions explored herein present chord-based Reynolds numbers ($Re_c$) beneath $4 \times 10^5$.

The utilization of multiple fidelity levels in this study allows for a pragmatic balance between computational cost and accuracy. To keep computational costs low for this investigation, the high-fidelity LBM is employed solely at TSR = 4 which gives an accurate in-depth analysis of the VAWT force and flow field. Additionally, taking advantage of faster computations for the mid-fidelity method, it is applied across a TSR spectrum from 1 to 7 which will allow exploring a wide range of operating conditions. This is anticipated to provide comprehensive insights into the VAWT fluid dynamic interactions arising from the presence of struts and a tower.

### D. Grid convergence setup

For the grid convergence study, the high-fidelity LBM is utilized to simulate the first VAWT configuration, comprising only the blades, across three distinct grid resolutions. Near the blade surface, VR regions are implemented with different voxel densities per chord for the resolutions termed 'Grid 1', 'Grid 2', and 'Grid 3'. The minimum and maximum voxel densities are designated to 'Grid 1' and 'Grid 3', respectively, with other VR region resolutions adjusted proportionally. Table 5 presents the y+ values and voxels per chord for each grid resolution. The y+ value, a non-dimensional parameter, represents the distance of the first cell centre from the computational domain wall in the wall-normal direction. This value is derived from the mean velocity value experienced by the blade at its mid-span location during a single rotation. The voxels per chord quantify the number of grid cells along the blade chord direction.

For the grid resolutions 'Grid 1' and 'Grid 3', the minimum voxel sizes are 0.826 mm and 0.413 mm, respectively. In the computational domain of the 2-bladed VAWT, 'Grid 1' comprises 7.06 million fine equivalent voxels, while 'Grid 3' encompasses 24.6 million. These fine equivalent voxels are obtained from the multiplication of the total voxel count with the time stepping rate, which is directly associated with the mesh resolution level. Evaluating the computational resource required, in terms of CPU hours needed for 12 rotor rotations (3.53 s), 'Grid 1' and 'Grid 3' configurations of the 2-bladed VAWT demand 3261 and 46380 CPU hours, respectively. These computations are executed on a Linux workstation, powered by an AMD Ryzen Threadripper 3990X Gen3 processor with 64 cores and a 128GB DDR4 3GHz platform. Notably, both the fine equivalent voxels and CPU hours exhibit similar values across all three VAWT configurations, with only a marginal increase for configurations including struts and tower. The physical time step for 'Grid 1' and 'Grid 3' corresponds to a Courant-Friedrichs-Lewy (CFL) number of 1 in the finest VR level and is $7.51 \times 10^{-6}$ s and $3.76 \times 10^{-6}$ s, respectively.

**Table 5 VAWT grid settings for the high-fidelity LBM simulation**

| | | Grid 1 | Grid 2 | Grid 3 |
|---|---|---|---|---|
| **First configuration - only blades** | y+ | 50 | 33.3 | 25 |
| | Voxels per chord | $9.1 \times 10^1$ | $1.36 \times 10^2$ | $1.81 \times 10^2$ |

## V. Results

### A. Temporal and grid convergence study

In this section, the temporal and grid convergence of the current VAWT setup is reported to check the reliability of the results. Firstly, temporal convergence is compared between the first two VAWT configurations for both aerodynamics and aeroacoustics. Secondly, grid convergence is investigated between different numerical grids for only the first VAWT configuration

*1. Temporal convergence*

Figure 3 depicts the statistical temporal convergence characteristics of the thrust coefficient ($C_T$) and torque coefficient ($C_Q$) for two VAWT configurations: the first configuration without any struts and tower, and the second configuration with struts and tower A. These coefficients are defined as:

$$C_T = \frac{T}{0.5\rho A V_\infty^2}, \tag{2}$$

$$C_Q = \frac{Q}{0.5\rho A V_\infty^2 R}, \tag{3}$$

where, $T$ and $Q$ are VAWT thrust and torque respectively, $\rho$ is the air density, $A$ is swept area ($D \times L$) where is $D$ is rotor diameter and $L$ is blade length. The results are obtained using both high-fidelity LBM (for the finest grid) and mid-fidelity LLFVW method. The corresponding uncertainty values ($u$) are calculated as a percentage of the standard deviation of thrust and torque values averaged over a complete rotation. These uncertainty values reflect the degree of uncertainty or variability in the computed thrust and torque coefficients over time due to the inherent unsteadiness and randomness in the fluid dynamic interactions.

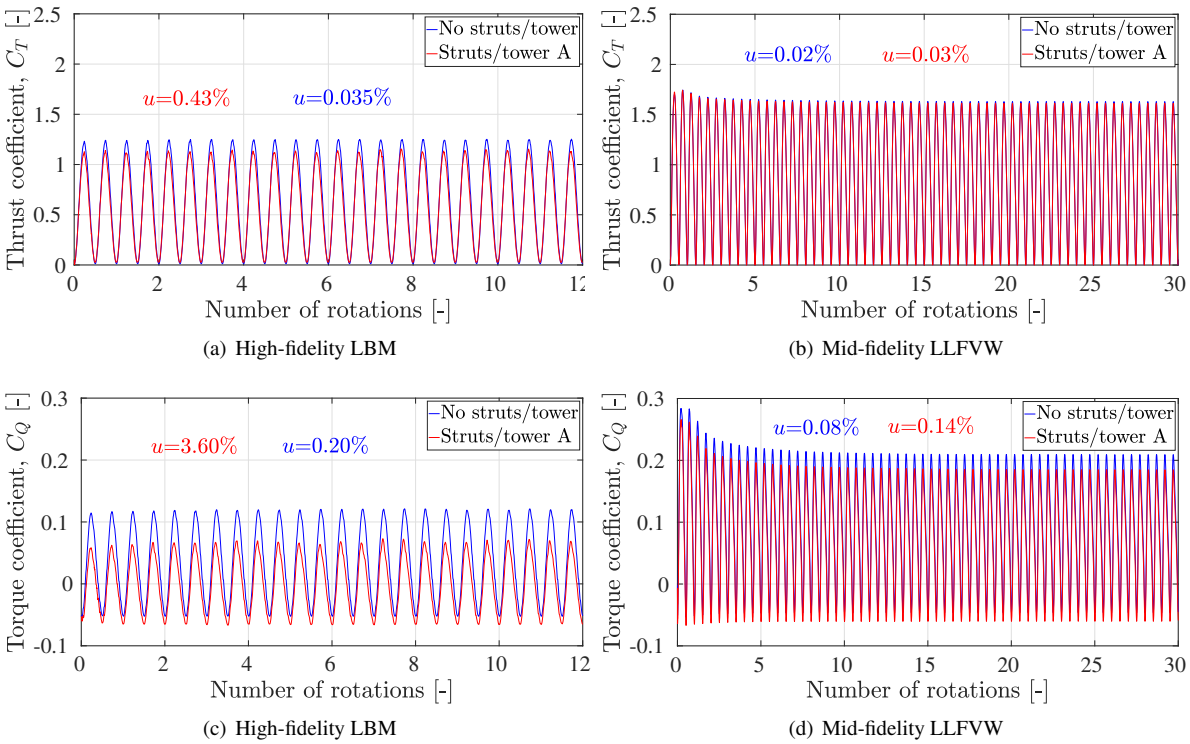


(a) High-fidelity LBM (b) Mid-fidelity LLFVW

(c) High-fidelity LBM (d) Mid-fidelity LLFVW

**Fig. 3 Statistical temporal convergence study for VAWT thrust coefficient $C_T$ and torque coefficient $C_Q$ using the high-fidelity LBM and mid-fidelity LLFVW for the finest Grid 3; the values are representative of the overall rotor**

All $u$ values depicted in the figures are calculated after the 10th rotor rotation for LBM and the 20th rotor rotation for LLFVW (the latter takes more rotations to reach convergence, as compared to the former). These specific time points are chosen to ensure a sufficient number of rotations for the simulation to reach a state of temporal stability and reliability, allowing for meaningful uncertainty assessment [67]. The reported values in the figures are representative of the overall rotor, comprising all blades and struts/tower (if present).

It is observed that temporal convergence is achieved at the same number of rotations when comparing the first and second configurations for any given parameter. This indicates that the presence of struts and a tower does not significantly influence the unsteady blade loading (since thrust and torque are directly derived from blade loading). A notable difference in the number of rotations required for convergence between thrust and torque values is evident when utilizing either of the two numerical methods. More precisely, regarding the $C_T$ values, convergence is attained after approximately 4 rotor rotations for LBM simulations and 10 rotor rotations for LLFVW simulations. Conversely, for the $C_Q$ values, temporal convergence requires roughly 6 rotor rotations for LBM and 15 rotor rotations for LLFVW simulations. Therefore, thrust values demonstrate faster convergence, as shown by the low uncertainty values ($u$), in contrast to torque values. This observation is consistent with previous studies on VAWTs operating at low Reynolds numbers [32, 68], further corroborating the present study outcomes.

Interestingly, these outcomes are contrary to those reported by Rezaeiha [69], wherein more than 20 rotations were necessary to attain temporal convergence in a high-fidelity CFD simulation using the incompressible Unsteady Reynolds-Averaged Navier-Stokes (URANS) method. It is pertinent to mention that in this study, the LBM simulations for the finer grid are initiated using the results from the coarser grid, which may have contributed to the reduced transient period. This seeding approach conforms to the current best practice for simulations of this type, where a coarser resolution is simulated first for a minimum of 10 rotor rotations. The final frame of this simulation is then used to seed a finer resolution simulation, which is executed with an initial settling time of a few blade-passage periods [48].

Figure 4 illustrates the temporal convergence of unsteady pressure data for the VAWT setup without struts and the central tower, using the high-fidelity LBM and the finest grid utilized in this study. Pressure data are sampled

at two distinct locations, both aligned along a line parallel to the VAWT rotational axis and positioned laterally at a distance of 2.6$D$, the precise coordinates being (0,0,2.6$D$) and (0.87$D$,0,2.6$D$). The analysis indicates that the temporal convergence is achieved after the 6th rotor rotation for both locations.

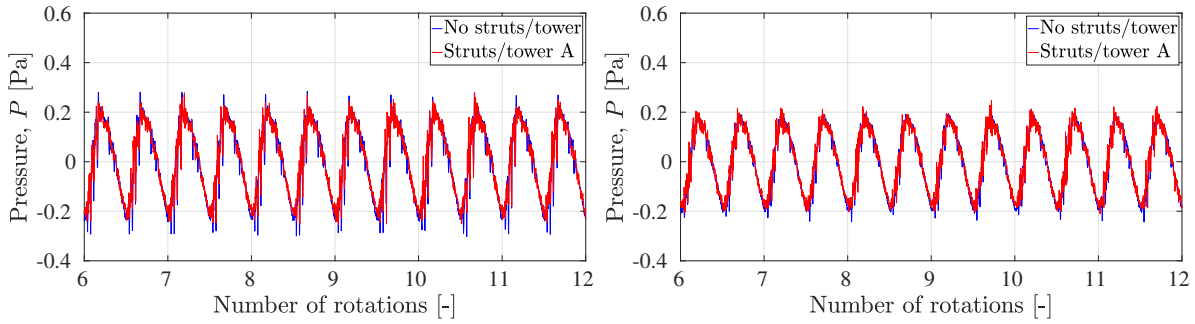


(a) At location (X,Y,Z)=(0,0,2.6$D$) (b) At location (X,Y,Z)=(0.87$D$,0,2.6$D$)

**Fig. 4 Statistical temporal convergence study for unsteady pressure data for the first configuration without struts and tower at TSR = 4, at two different locations using the high-fidelity LBM for the finest grid 3**

Consequently, keeping in mind the temporal convergence of both aerodynamics and aeroacoustics, all subsequent results presented are based on data acquired after the 6th rotor rotation for the LBM and the 15th rotation for the LLFVW methodology.

*2. Grid convergence*

Figure 5 illustrates the results of the grid convergence analysis for the first VAWT configuration without the struts and central tower. The figure shows the fluctuation of the phase-locked normal force coefficient ($C_{Fn}$) spanning three different numerical grids employed in the LBM simulations, over a single 360° rotation for a single blade. The data presented contains the sum of contributions of all points on the blade. Such an investigation is essential to understand the independence of the derived results from the chosen numerical grid, thereby affirming the robustness and accuracy of the simulations. The findings indicate that the normal forces exhibit satisfactory agreement between grid 2 and grid 3, covering both the upwind and downwind segments of the rotor rotation.

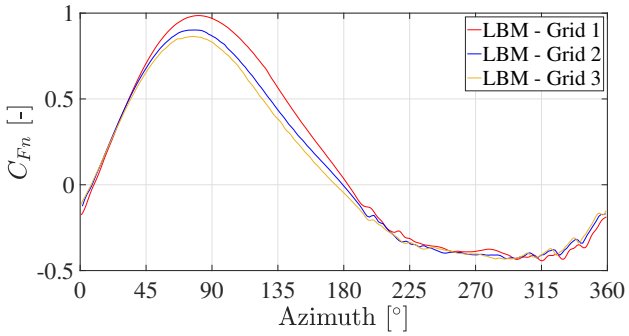


**Fig. 5 Grid convergence study for phase-locked VAWT normal force coefficient $C_{Fn}$ of a single blade, using the high-fidelity LBM for TSR = 4**

The grid convergence for mean $C_T$ and $C_Q$ values has been investigated for the first VAWT configuration, as shown in Figure 6. The values represent the entire rotor, encapsulating both blades of the VAWT. The resolution of the grid is characterized by the grid spacing ($h$), normalized with the blade chord ($c$). Notably, $h$ denotes the smallest grid (voxel) dimension within the computational domain. Additionally, the figure shows the values obtained via the Richardson extrapolation technique [68], which calculates the value of $C_T$ and $C_Q$ as $h/c \rightarrow 0$. This extrapolation physically symbolizes the approach towards the continuum threshold, wherein an infinite number of cells is utilized in the Cartesian

grid. Furthermore, the Grid Convergence Index (GCI) (calculation of GCI is mentioned in previous studies [68, 70]) for each respective case is listed, based on the variation between successive grid resolutions [68, 70] and is an important parameter for estimating the potential error in the solution.

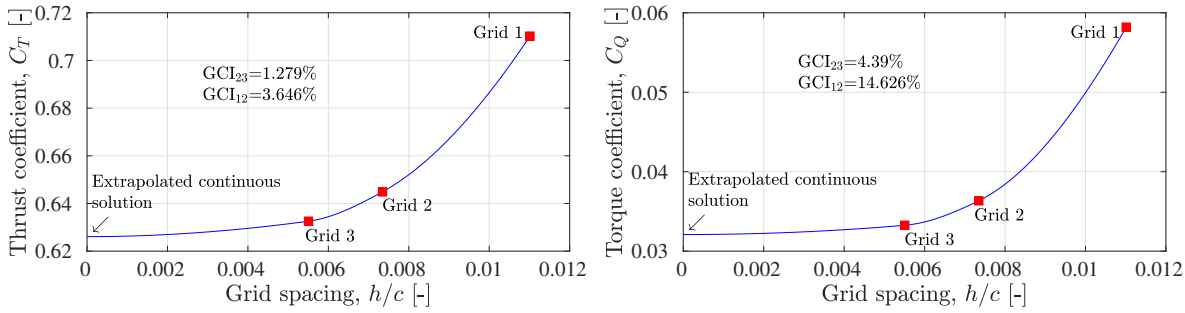


(a) Thrust values

(b) Torque values

**Fig. 6 Grid convergence study for VAWT thrust coefficient $C_T$ and torque coefficient $C_Q$ for the first configuration without struts and tower, using the high-fidelity LBM at TSR = 4**

The findings show that $C_T$ has smaller GCI values than $C_Q$, suggesting that a relatively coarser grid resolution suffices to capture converged blade loading values. In contrast, a more refined resolution is required to attain converged blade torque (or power) values. This behaviour can be attributed to the higher sensitivity of skin friction and drag values to the y+ values of different grids. The accurate estimation of airfoil drag across both low and high Reynolds number flows remains an active research field [71]. For the current VAWT configuration, GCI23 consistently remains smaller than GCI12 for both $C_T$ and $C_Q$, a pattern also found in a previous study [32] when the number of blades is varied. This implies that increasing the grid resolution can lead to more precise and reliable results since the differences related to the numerical grid diminish, enhancing the accuracy of the simulations. Nonetheless, it is imperative to acknowledge that the relative GCI values might exhibit significant variations in VAWT simulations, depending on factors such as the simulated tip speed ratio and rotor scale [68].

Furthermore, findings from a previous investigation by Shubham et al. [68], utilizing a similar VAWT numerical setup as the current study, revealed that the grid convergence of the Overall Sound Pressure Level (OSPL) (not presented to avoid too many figures) is comparable to that of thrust values and superior to torque values. This aligns with the fact that, in the context of VAWTs operating at low Reynolds numbers, loading noise has the most significant contribution to the overall noise [72]. Consequently, given the favourable convergence observed for grid 3, it is prudent to select this grid resolution for all subsequent numerical simulations. It is deemed sufficient to enable an accurate and insightful physical analysis of the fluid dynamic interactions and noise sources in the VAWT.

### B. Aerodynamics

Figure 7 shows phase-locked $C_{Fn}$ variation for a single blade throughout its complete rotation. The figure shows the results from grid 3 of the present high-fidelity LBM setup, the mid-fidelity configuration, a reference high-fidelity simulation [43], and experiments [63, 64]. The label 'Experiment - clean' pertains to results without any boundary layer (BL) trip, whereas 'Experiment - trip' is with the BL trip positioned at 15% chord, on both the pressure and suction sides of the airfoil, to force flow transition.

The results exhibit some differences between the LBM simulations of the present study (first configuration without struts/tower), the benchmark LBM simulation, and the experimental study without the BL trip, especially in the upwind part of the rotor rotation. In the downwind part, a difference is observed around the most downstream position (270°) amongst the previously mentioned LBM results. The BL trip is expected to cause a marked increase in blade loading within the reference LBM simulation, particularly evident in the downwind part. Both the mid-fidelity LLFVW results show fairly good agreement with the reference LBM results, in the upwind part of the rotation, although a mismatch is observed in the downwind part.

In both the upwind and downwind parts of rotation, the absolute magnitudes of $C_{Fn}$ as predicted by LBM are consistently lower than that by the LLFVW method, irrespective of the presence or absence of struts/tower. This difference arises from the level of physical realism in modelling the induction effects in both methods. The LLFVW

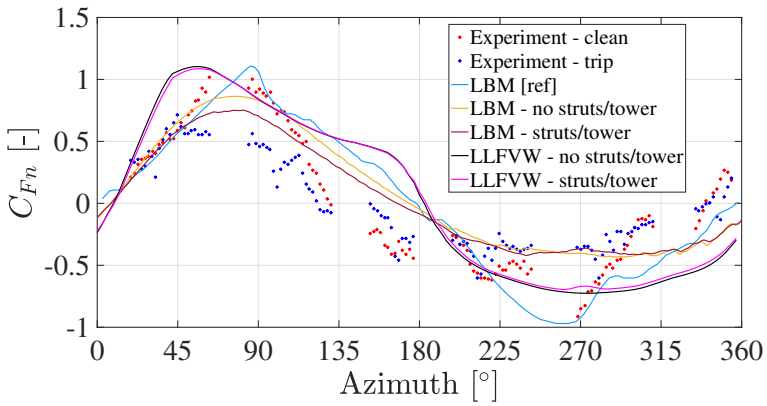


**Fig. 7 Phase-locked normal force coefficient $C_{Fn}$ of a single blade using high-fidelity LBM and mid-fidelity LLFVW of first two configurations, compared with experimental ('clean' without BL trip, 'trip' with BL trip) and reference high-fidelity LBM results (LBM [ref]), at TSR = 4**



method employs a simplified representation of the flow field using vortex lines and Biot-Savart law to determine the induced velocities. This approach may not fully account for the dynamic interaction between the blades and the wake, particularly in the downwind part of the rotor where the flow is highly 3D and unsteady. In contrast, the LBM inherently accounts for the full range of flow physics, including turbulence, vortex shedding, and dynamic stall, which occur in the VAWT flow field. This method provides a more accurate representation of the flow induction, as it naturally incorporates the reduction in local flow velocity due to the aerodynamic blockage and wake formation caused by the blades. Consequently, LLFVW may predict higher local flow velocities due to its simplified induction model, relative to LBM and therefore larger value of normal blade forces.

Furthermore, in the context of LBM, the addition of struts and a central tower results in a reduction in blade loading in the upwind part. Conversely, the loading remains relatively unchanged in the downwind part, except for a slight decrease around the azimuth of 270°, directly downstream of the central tower. This downstream effect is also well represented by the LLFVW results, though the difference observed in the upwind part due to the struts and tower remains negligible. As a whole, the validation of both the mid-fidelity and high-fidelity setups employed in this study is deemed satisfactory. These validated setups can be effectively employed for an in-depth exploration of VAWT fluid dynamic interactions and wake dynamics, offering valuable insights into the intricacies of VAWT performance.

Figure 8 depicts the instantaneous streamwise velocities encountered by the cross-sectional airfoil at various azimuth positions, as obtained using the high-fidelity LBM. These findings can be compared with those reported by Brandetti et al. [43] in Figure 9. Across all azimuth positions, the BL trip induces more prominent flow separation in the latter, as compared to the present study. This leads to differences in blade loading, both in the upwind and downwind parts of rotation, as evident in Figure 7.

It is imperative to note that the ratio of BL trip height to chord length ($t/c$) employed in both the benchmark LBM simulation and experiment stands at 0.0067 (equivalent to $t$ = 0.5 mm), much higher than the values adopted for VAWTs or alternative rotor types (0.0027 as per Pearson [73] with $t$ = 0.15 mm and 0.003 as per Weber et al. [74] with $t$ = 0.15 mm). The increased BL trip height might have resulted in its role as a bluff-body/step in the flow over the NACA 0021 airfoil, rather than serving its designated function of forcing flow transition from laminar to turbulent regimes. Furthermore, the BL trip has to be optimized for all different azimuthal locations, since it has been shown to be effective only for certain azimuthal locations and not all of them [43]. This is because the blade experiences different blade-effective velocities along the rotation. Such observations highlight the sensitivity of VAWT aerodynamics to BL trip configurations, underscoring the need for subsequent studies to investigate their optimized design and chordwise positioning on VAWT blades.

Figure 10 presents the computed values of mean $C_P$ and $C_T$ for the three different VAWT configurations used in this chapter. The mid-fidelity LLFVW simulations encompass the entire spectrum of TSRs, whereas the high-fidelity LBM simulations are specifically undertaken for a TSR of 4. The mid-fidelity data suggests that struts and tower influence VAWT performance. Across all TSRs, introducing struts and tower (for both towers A and B) diminishes the $C_P$ and $C_T$ values, especially at higher TSRs. At lower TSRs, blades function more independently, with limited

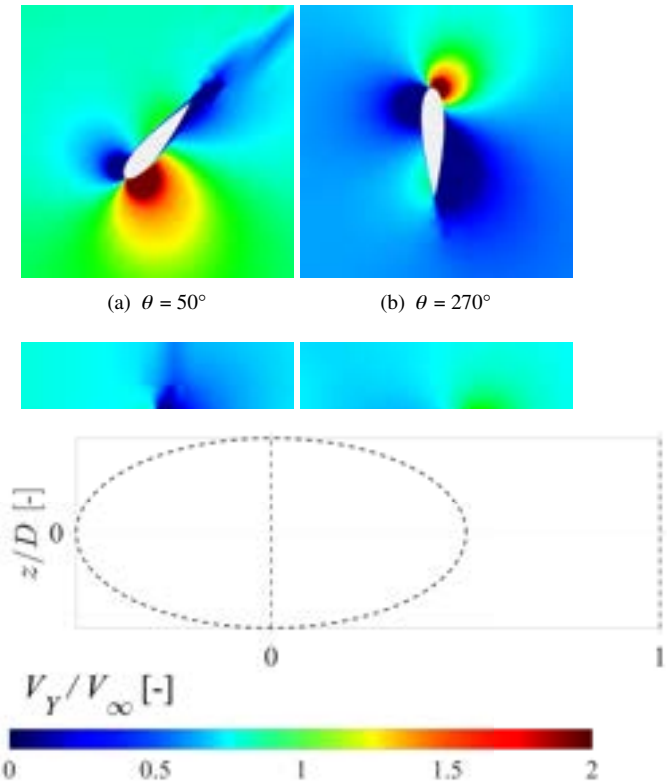


**Fig. 8 Instantaneous streamwise velocities experienced by a VAWT blade at different azimuth locations for the VAWT configuration without struts and tower, using the high-fidelity LBM at TSR = 4**

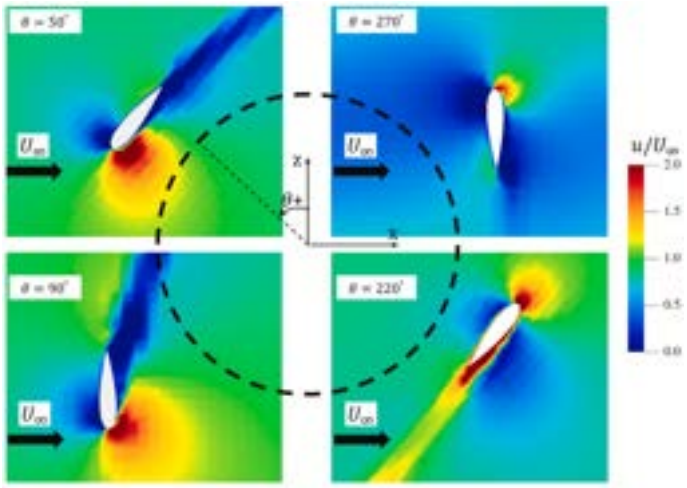


**Fig. 9 Instantaneous streamwise velocities experienced by a VAWT blade at different azimuth locations as obtained by Brandetti et al. [43]; $u$: streamwise velocity, $U_\infty$: freestream velocity (reprinted after written permission)**

blade-wake/blade-vortex interaction (BWI/BVI) due to added support structures, causing minor reductions in $C_P$ and $C_T$. As TSR rises, so does the induction factor and the significance of BWI/BVI. The presence of these support structures intensifies these fluid dynamic interactions, leading to decreased blade loading and overall rotor power and thrust. For the same reason, higher TSRs show a steeper $C_P$ gradient than lower TSRs. The VAWT self-starting capability ($C_P$ at very low TSR) remains largely unaffected by the addition of struts and tower, but a pronounced impact is observed for

the $C_P$ at the optimal TSR (TSR = 4 here). On the other hand, the optimal TSR value remains unchanged even after the addition of support structures.

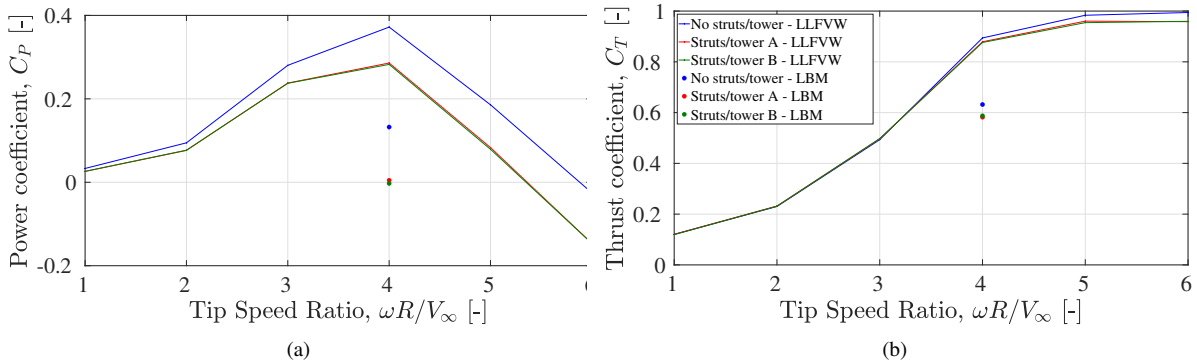


**Fig. 10 Mean power and thrust values obtained for the three VAWT configurations using the mid-fidelity LLFVW and high-fidelity LBM; line represents mid-fidelity and dot represents high-fidelity results**

The thrust coefficient ($C_T$) displays an asymptotic behaviour with increasing TSR across the three VAWT configurations. The inclusion of struts and tower influence $C_T$ values minimally (by 0.5% - 1.6%), with deviations slightly increasing after the TSR value of 3.5 (by 3% - 3.6%). Conversely, $C_P$ reductions are large even at lower TSRs (15% - 21%) going even higher in the range of 40% - 55% at higher TSRs. This indicates an increased sensitivity of tangential blade loading (affecting $C_P$) to these support structures as compared to normal loading (affecting $C_T$). Additionally, enlarging tower diameter from tower A to tower B reduces both $C_P$ and $C_T$ values, but the magnitude of this reduction is found to be relatively insignificant (0.5% - 3%).

Comparing mid-fidelity LLFVW to high-fidelity LBM at TSR 4 shows differences in $C_P$ (19%) and $C_T$ (10%). These differences increase with the inclusion of struts and a central tower. For the VAWT without struts and tower, the $C_P$ difference between mid and high-fidelity is 0.24 (19%), but increases to 0.281 (30%) and 0.285 (31%) for the second and third VAWT configurations, respectively, when struts and tower are introduced. Remarkably, power generation becomes negative for the third configuration featuring tower B. A similar pattern is exhibited by $C_T$ values, where the difference between LBM and LLFVW results grows with strut and tower additions (from 10% to 19%).

Figure 11 illustrates the $C_T$ and $C_Q$ fluctuations for a single blade over a full 360° azimuth at TSR = 4, comparing both methods. It also highlights the mean values for the rotation. The data reveals a decline in $C_T$ and $C_Q$ due to struts and tower, evident in both upwind and downwind rotations. This drop results from increased BWI/BVI with the addition of support structures, diminishing the blade's aerodynamic efficiency. The downstream blade exhibits reduced thrust and torque values than the upstream ones, with a marked decrease near the 270° azimuth, directly downstream of the central tower. This performance decrease amplifies with a broader tower diameter, leading to decreased average rotor thrust and torque, as shown in Figure 10.

The findings also reveal negative torque generation for a substantial portion of the rotation, especially apparent with LBM results with struts and a tower, underscoring the degrading effect of the added support structures. Both mid-fidelity LLFVW and high-fidelity LBM exhibit the same trend observed in the azimuthal variation of $C_T$ and $C_Q$. Yet, a comparison of $C_T$ and $C_Q$ values reveals that LLFVW consistently predicts higher $C_T$ and $C_Q$ values than LBM throughout the rotation. LBM also shows a higher decline in blade performance than LLFVW, with the latter displaying only minimal differences in the upwind rotation segment. Another observation is the limitation of the LLFVW method to capture the reduction in blade performance from upwind to downwind part of the rotation. In this context, LLFVW predicts a lower reduction in thrust and torque values as compared to LBM, which shows that the former is unable to capture the complex 3D fluid dynamic interactions prevalent in the downwind part of rotation. Consequently, LLFVW predicts higher thrust and torque values than LBM.

It is important to note that XFOIL polar values ($C_l$ and $C_d$ vs angle of attack $\alpha$) are utilized in the analytical formulation of LLFVW, which influence the blade angle of attack and induced velocity, and this has a significant impact on the thrust and torque values obtained. It is suggested to modify these polars accordingly by introducing empirical corrections in future investigations [35, 75]. An alternative approach involves using airfoil polar values for 360° angle of attack obtained through wind tunnel experiments [76, 77].

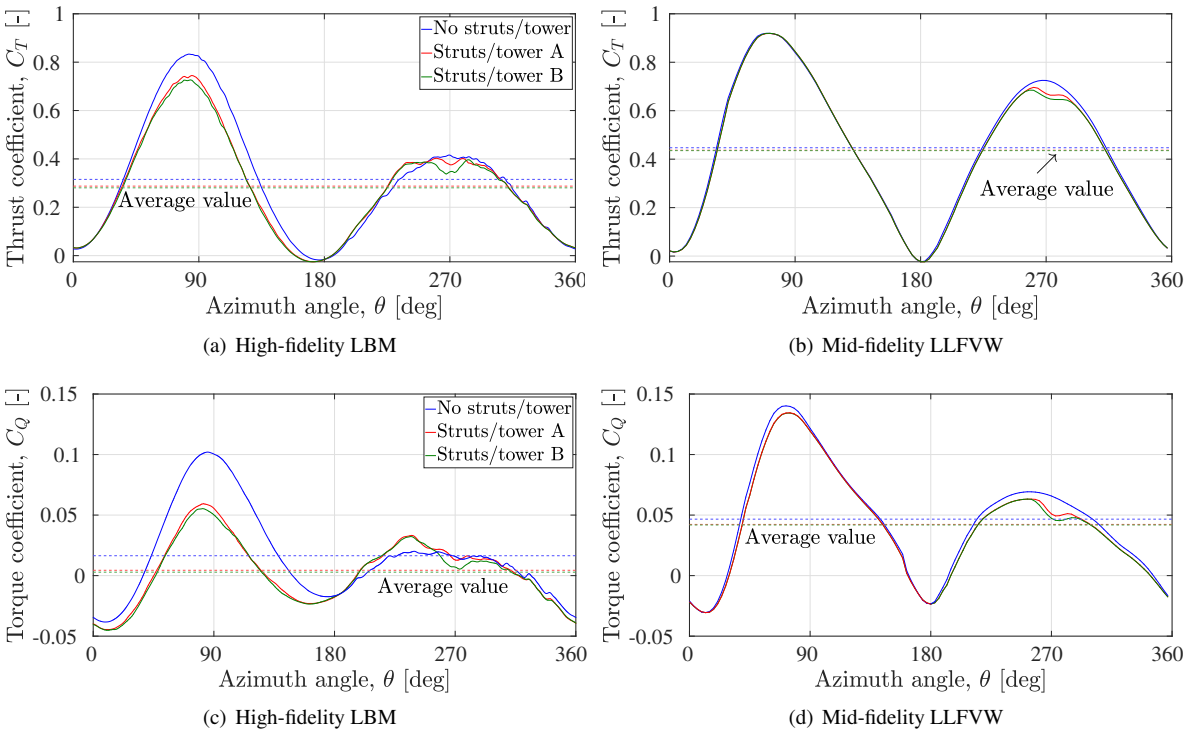


(a) High-fidelity LBM (b) Mid-fidelity LLFVW

(c) High-fidelity LBM (d) Mid-fidelity LLFVW

**Fig. 11 Variation of thrust coefficient $C_T$ and torque coefficient $C_Q$ for a single blade over a complete rotation, using the high-fidelity LBM and mid-fidelity LLFVW at TSR = 4**

The above-mentioned unsteady force field characteristics can also be visualized from Figure 12 which illustrates the variation in blade normal forces ($F_n$) over the 3D cylindrical surface traced by VAWT blades at TSR = 4. When comparing azimuthal and spanwise values across VAWT configurations between LBM and LLFVW, several observations emerge. Normal blade forces show a decline in the downwind rotation segment compared to the upwind, a trend consistently captured by both numerical methods across all VAWT configurations. This loading fluctuation is inherent to VAWTs and is a consequence of the complex blade-wake/blade-vortex interactions.

Additionally, the struts positioned at $h/H$ of 0.26 and -0.26 influence the spanwise blade loading distribution. Particularly in the upwind rotation, these struts lead to a noticeable loading deficit, resulting in reduced overall blade loading as observed in Figure 11. However, their effect reduces in the downwind part, where the blade loading is more reduced and unsteady in nature, as compared to the upwind part. Notably, the mid-fidelity simulation does not capture this strut effect. This behaviour might arise from the symmetrical airfoil used for the struts with a zero angle of attack, preventing any vortex line shedding from the lifting line of the strut blades, causing no observed effect in the spanwise blade loading in the mid-fidelity simulation.

Both mid-fidelity and high-fidelity results underscore the central tower effect, especially in the downwind rotation segment. The presence of the tower results in a blade loading deficit, most notable at the 270° azimuth downstream location. A wider tower diameter intensifies this deficit, leading to the observed dip in thrust and torque values in Figure 11. Notably, LLFVW consistently predicts higher blade loading values throughout the rotation compared to LBM. This difference is reflected in the individual blade thrust and torque values, as depicted in Figure 11. Furthermore, LBM more distinctly captures the 3D effects of tip vortex on the force field, apparent around $h/H$ of -0.5 and 0.5 in Figure 12. These observations show that while mid-fidelity vortex methods capture general trends in VAWT performance, they have limitations in accurately capturing the 3D blade vortex interactions and their effect on VAWT force field, especially amidst support structures like struts and tower, as compared to the high-fidelity LBM approach.

To get deeper insight into blade-wake and blade-vortex interactions, Figure 13 depicts the instantaneous vortices in the downstream region of the VAWT flow field, using iso-surfaces of the $\lambda_2$ criterion. Coherent tip vortices, shedding from each blade tip, travel downstream, forming a distinct "vortex ring" spiral pattern around the turbine's axis. This convective motion of the large vortex structures is accompanied by wake expansion, eventually fragments into smaller

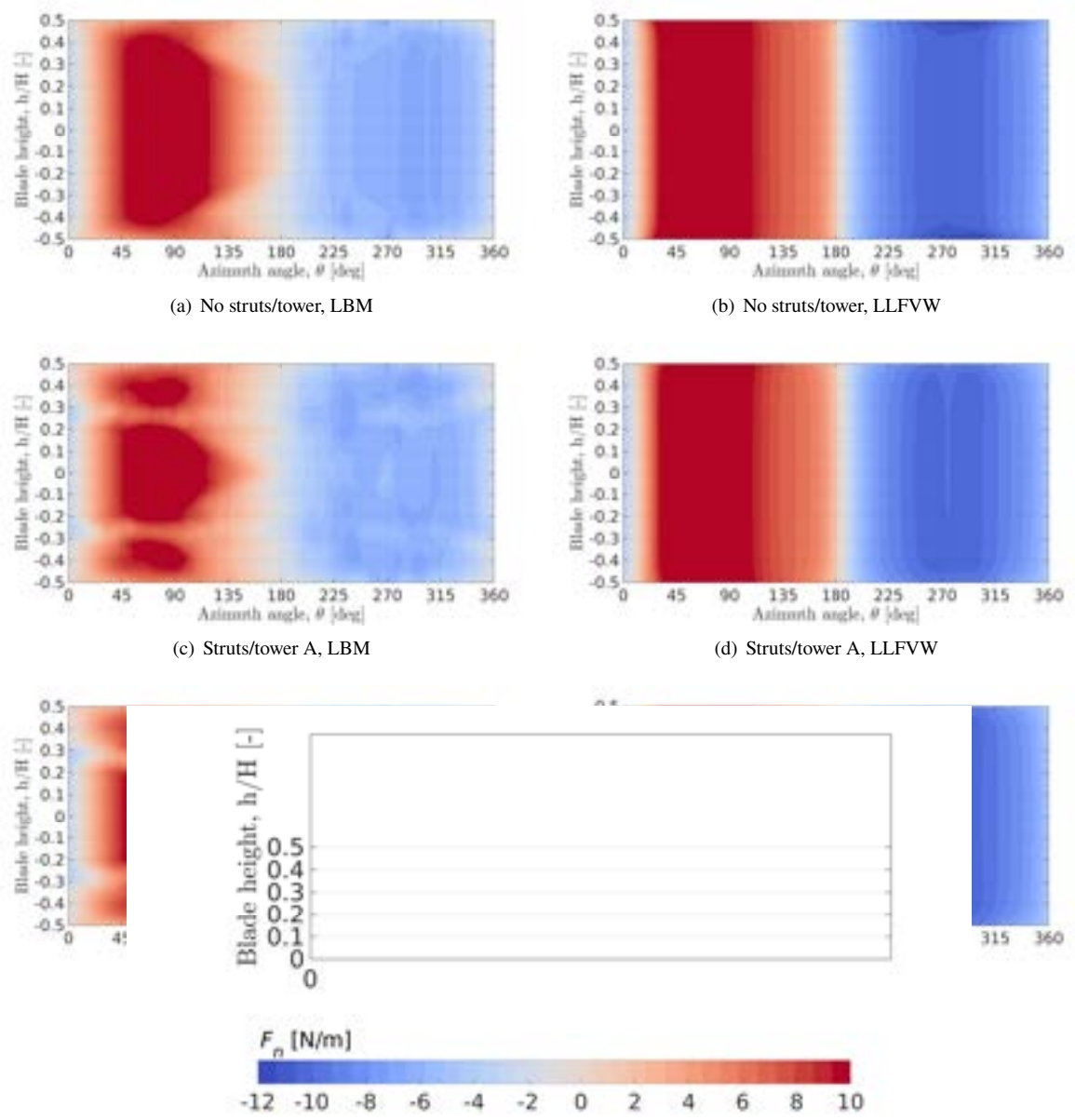


(a) No struts/tower, LBM

(b) No struts/tower, LLFVW

(c) Struts/tower A, LBM

(d) Struts/tower A, LLFVW

**Fig. 12 Normal force contour for a single blade over azimuthal and spanwise directions, using the high-fidelity LBM and mid-fidelity LLFVW, at TSR = 4**

structures due to flow instabilities and spatial modulation, which then disperse and merge with the surrounding fluid [78, 79]. Notably, the presence of struts and a central tower amplifies the presence of these fragmented smaller vortex structures. This enhancement in BWI/BVI disrupts optimal pressure and loading distribution across the blade, resulting in reduced blade loading upon the addition of struts and a tower. Such findings are consistent with data from Figures 11 and 12, underscoring the significant influence of struts and a tower in affecting VAWT performance.

These findings indicate that the mid-fidelity method might not effectively capture the complex 3D effects in a VAWT flow and force field, especially in the near-wake region with pronounced BWI/BVI, as effectively as the high-fidelity method does. Such discrepancies are not unexpected, given the inherent differences in fluid modelling approaches between the two methods. However, it is noteworthy that the trends in mean and azimuthal variation of $C_P$ and $C_T$ observed by the mid-fidelity LLFVW method align with the LBM results at TSR = 4, in Figure 10, where introducing

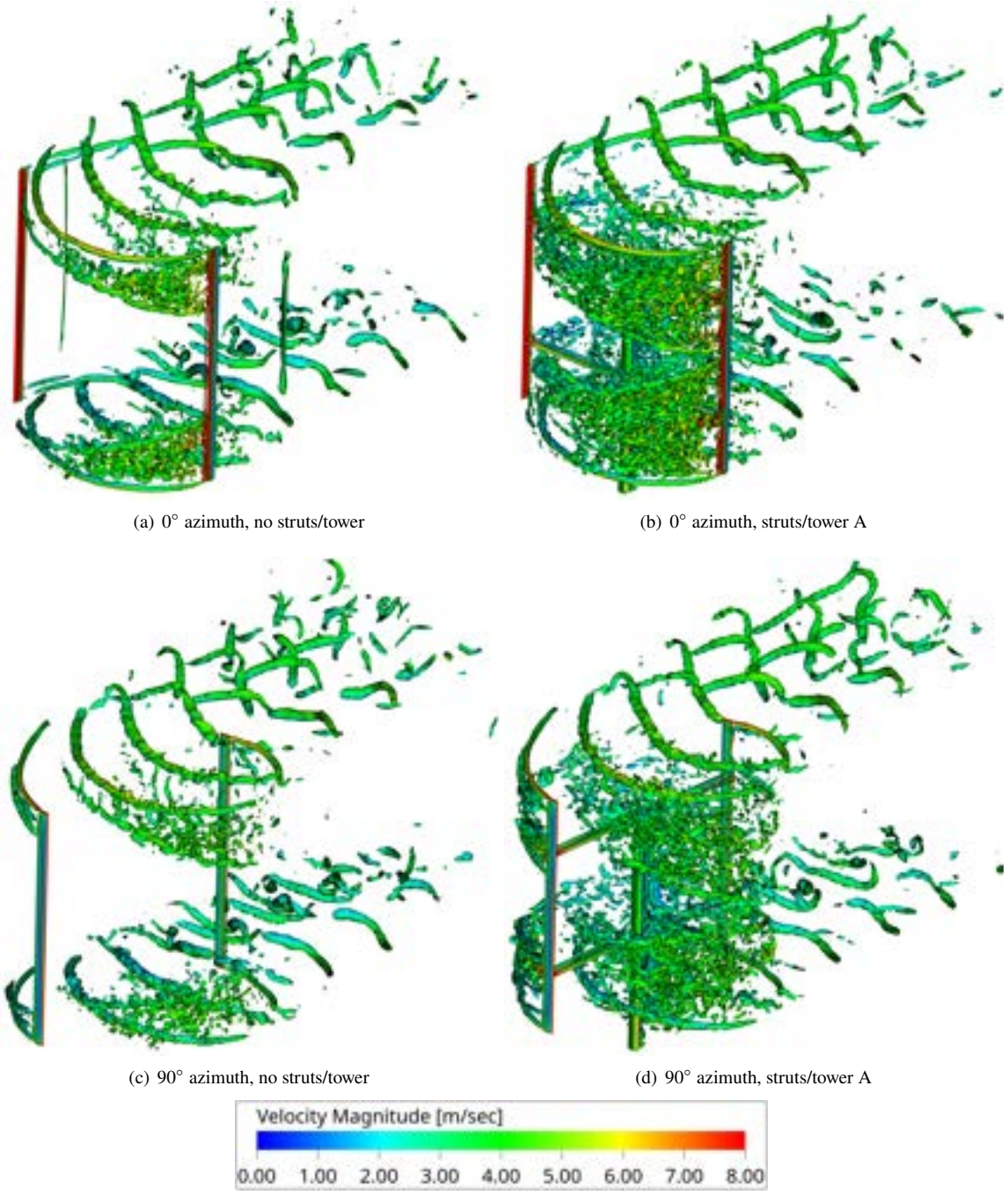


(a) 0° azimuth, no struts/tower

(b) 0° azimuth, struts/tower A

(c) 90° azimuth, no struts/tower

(d) 90° azimuth, struts/tower A

**Fig. 13 Instantaneous 3D flowfield using iso-surfaces of the $\lambda_2$ criterion for vortices visualization, using high-fidelity LBM at TSR = 4**

struts and tower reduces power and thrust values.

Figure 14 shows the instantaneous streamwise velocity contours within the VAWT wake on a mid-span 2D plane, contrasting results from LBM and LLFVW at TSR = 4. The increased VAWT wake strength due to the presence of struts and tower can be observed, although the difference is minimal. The central tower causes an added velocity deficit downstream, correlating with the reduced blade loading around the 270° azimuth, as shown in Figures 11 and 12.

As the tower gets wider (tower A → tower B), the velocity deficit increases, which is expected to increase BWI/BVI due to the vortices shed from the tower, thereby altering wake dynamics. Both simulation methods depict this influence

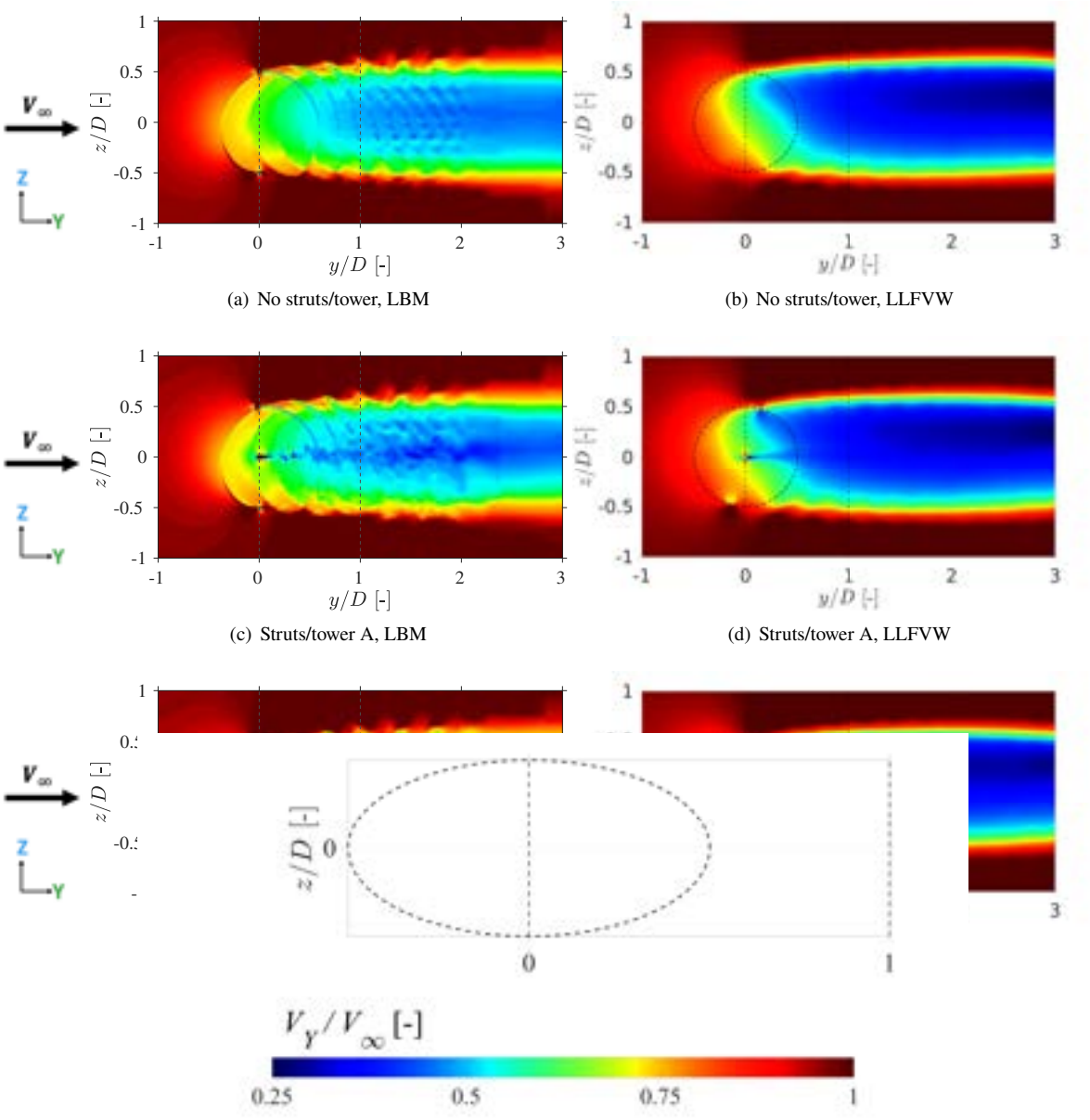


(a) No struts/tower, LBM

(b) No struts/tower, LLFVW

(c) Struts/tower A, LBM

(d) Struts/tower A, LLFVW

**Fig. 14 Instantaneous streamwise velocity contours in the VAWT wake on a 2D plane located at the blade mid-span location, using both LBM and LLFVW methods, at TSR = 4**

of the central tower, but notably, LLFVW consistently predicts reduced wake velocities across all VAWT configurations when compared with LBM. A stronger force distribution on an airfoil or blade typically exhibits a stronger downstream wake, marked by increased velocity deficits and vortex structures. This is in line with the increased rotor thrust values LLFVW predicted relative to LBM, as illustrated in Figure 11. Furthermore, the 2D vortex patterns in Figure 14 from LBM are more distinct than the LLFVW results. Such patterns signify shed vortices, as observed in the 3D representation in Figure 13. These vortical structures underscore the dissimilarity in vortex modelling approaches between the two methods, with LBM showing a more accurate capture of blade vortex interactions than the LLFVW method.

Figure 11 illustrated that the inclusion of struts and a central tower has a lower impact on blade loading in the downwind part of rotation than in the upwind part. Figures 13 and 14 exhibit some observable increase in BWI/BVI due to struts/tower, but for the downwind part, it does not cause a substantial effect on blade loading. This can be attributed to the presence of a strong BVI already occurring in the downwind region when only the blades are present within the

VAWT flowfield. Conversely, in the upwind part of rotation, when only the blades are present, the BVI is minimal but gets more pronounced due to the presence of struts and central tower, resulting in a significant change in blade loading.

The differences in wake velocities between the two numerical methods are further investigated quantitatively in Figure 15, showing streamwise velocity values averaged over an entire rotation for the three VAWT configurations. These velocities are sampled along lines positioned $0D$ and $1D$ downstream from the VAWT centre on the blade mid-span 2D plane, denoted by black dotted lines in Figure 14. On the centreline of the VAWT ($y = 0D$), LLFVW predicts increased streamwise velocities relative to LBM. This supports the previous argument on higher blade loading for the former than the latter in Figures 7, 10 and 11. In contrast, at the $1D$ downstream location, LLFVW predicts reduced streamwise velocities compared to LBM. It is worth noting the inherent asymmetry of the VAWT flow field across all configurations, especially pronounced in the LLFVW results.

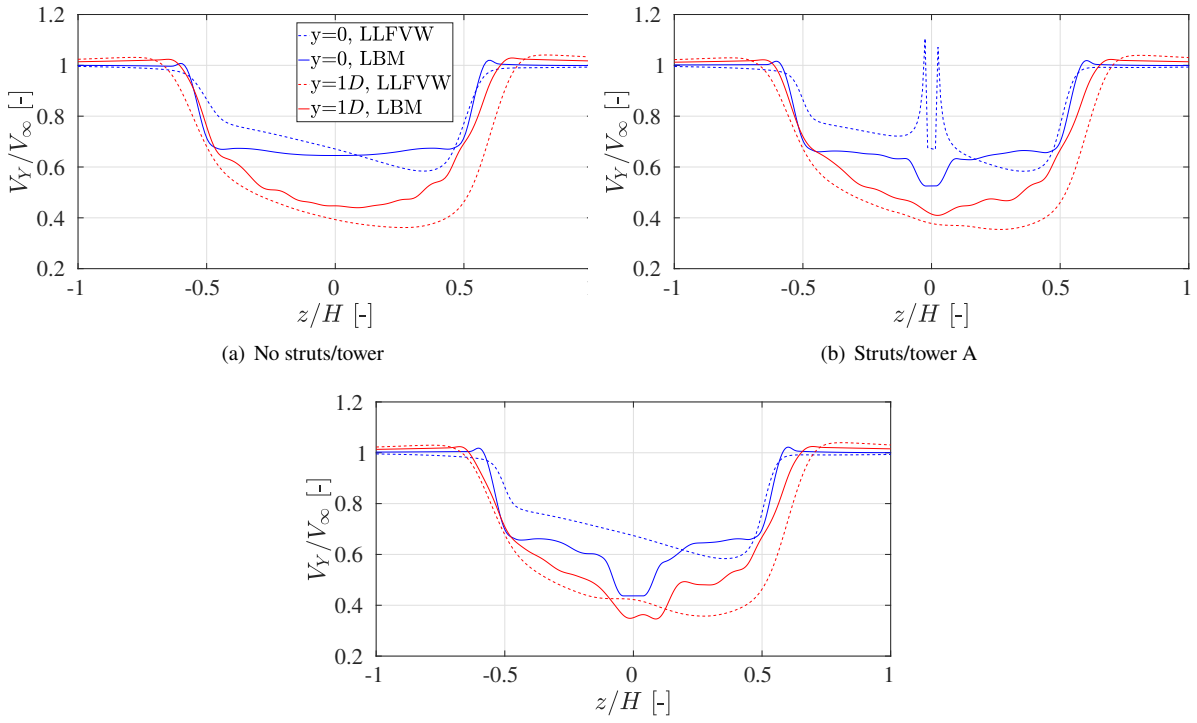


(a) No struts/tower

(b) Struts/tower A

(c) Struts/tower B

**Fig. 15 Comparison of streamwise velocities, averaged over a rotation, in the downstream VAWT flowfield using high-fidelity LBM and mid-fidelity LLFVW at two different downstream locations, at TSR = 4; the x-axis in the figures is in the lateral/cross-streamwise direction**

Figure 16 presents the unsteady pressure data sampled over a single rotor rotation at two specific points: on the rotor plane (0,0,2.6$D$) and outside the rotor plane (0.87$D$,0,2.6$D$). This dataset encompasses contributions from the blades and, where present, struts and central tower. Firstly, comparing these two locations, the out-of-plane location exhibits reduced high-frequency pressure fluctuations relative to the in-plane location. Secondly, the addition of struts and a central tower results in only a marginal increase in unsteady pressure fluctuations, particularly at the in-plane location, aligning with the observations from Figure 3 for the temporal convergence behaviour. Notably, all three VAWT configurations display pronounced pressure drops around 30°, 45°, and 60° azimuths, likely due to downstream blade interactions with the vortices shed by the upstream blades in the wake.

To gain deeper insights into the effect of struts and tower on noise generation, the noise spectra of all three VAWT configurations are analyzed. Figure 17 presents the Sound Pressure Level (SPL) values in dB/Hz spanning 20-2000 Hz at the two observer points. Introducing struts and tower increases SPL values for frequencies above ≈300 Hz at both locations, a consequence of heightened BWI/BVI, as visualized in Figure 13. However, for the low-frequency range (50-200 Hz), SPL values diminish with the inclusion of these support structures, correlating with the reduced integral blade loading seen in Figure 11. This reduced tonal component of blade loading noise yields decreased SPL values

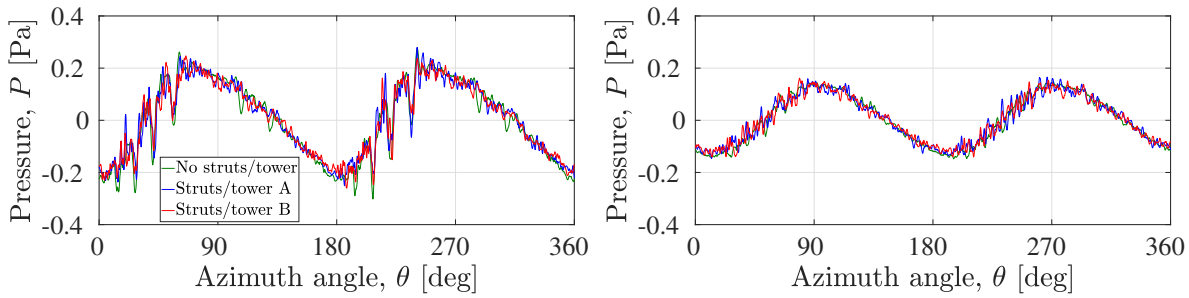


(a) At X,Y,Z = (0,0,2.6$D$) (b) At X,Y,Z = (0.87$D$,0,2.6$D$)

**Fig. 16 Sound Pressure Level (SPL) spectra using the high-fidelity LBM at two different locations, at TSR = 4**

at these frequencies. Notably, this effect is more pronounced for the in-plane location, where the influence of blade loading on the tonal component is most significant. Consistent with Figure 16, the in-plane location exhibits higher noise levels across all frequencies compared to its out-of-plane counterpart.

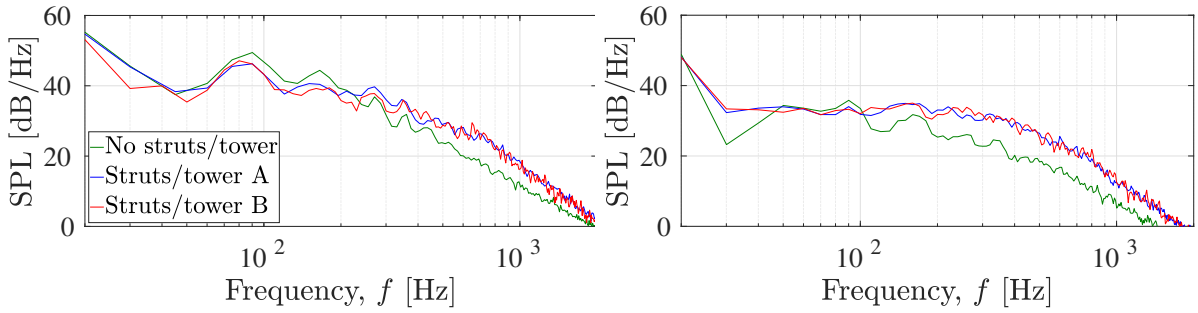


(a) At X,Y,Z = (0,0,2.6$D$) (b) At X,Y,Z = (0.87$D$,0,2.6$D$)

**Fig. 17 Sound Pressure Level (SPL) spectra using the high-fidelity LBM at two different locations, at TSR = 4**

## VI. Conclusions and Recommendations

The present research performs an in-depth investigation into the aerodynamics and aeroacoustics of VAWTs to understand the effects of incorporating supporting struts and a central tower into the setup. The LBM is employed for high-fidelity aerodynamic simulations, complemented by aeroacoustic post-processing via the FW-H approach for far-field noise estimation. Additionally, mid-fidelity aerodynamic simulations are performed utilizing the Lifting Line Free Vortex Wake (LLFVW) method. A straight-bladed Darrieus VAWT is utilized with 2 blades and three distinct VAWT configurations are simulated. The rotor diameter is 1.5m and the solidity is 0.1. The first configuration is a simple 2-bladed VAWT, the second configuration integrates four supporting struts and a central tower with the blades, and the third configuration increases the central tower diameter to double that of the second configuration.

It is observed that the number of rotations required for statistical temporal convergence does not vary between the first two VAWT configurations. Thrust values converge in only 4 rotor rotations with reduced uncertainty while torque values take 10 rotations, for high-fidelity LBM. Furthermore, grid convergence analysis also shows that thrust requires a coarser grid to converge than torque. The study reveals a reduction in mean power and thrust across all TSRs as a consequence of the presence of struts and a tower, although the effect on the latter (3% - 3.6%) is much less than the former (15% - 55%). The addition of these structures degrades the tangential and normal loading on each blade and overall rotor performance, with struts particularly worsening the spanwise force distribution. This effect becomes severe as TSR increases.

Azimuthal thrust and torque values are reduced by the presence of struts and a tower during both the upwind and downwind parts of rotation, attributable to increased blade-wake and blade-vortex interactions (BWI/BVI) caused by these support structures. A notable reduction in blade loading is observed around the 270° azimuth, directly downstream

of the central tower. This happens due to the tower wake, the strength of which increases with tower diameter, further reducing blade loading. Notwithstanding these effects, the inclusion of struts and tower does not compromise the VAWT self-starting capabilities ($C_P$ at very low TSR) or the optimal TSR, although it does result in a reduced optimal power output.

The comparative analysis of the mid-fidelity LLFVW and high-fidelity LBM results proves their effectiveness in capturing the physical phenomena arising due to struts and a tower. Nonetheless, the LLFVW results consistently estimate higher thrust and torque values across the upwind and downwind parts of rotation relative to the LBM, a pattern that is reflected also when calculating the mean thrust (higher by 10%) and torque values (higher by 19%) and evaluating the normal forces on individual blades for all VAWT configurations. This suggests a potential drawback of the LLFVW method in fully capturing the complex 3D effects within the VAWT flow and force fields, particularly in configurations inclusive of struts and a tower. As a result, the LLFVW predicts higher integral thrust and power for the rotor as a whole in comparison to the LBM. Due to increased blade loading, streamwise wake velocities predicted were lower by the LLFVW method, contributing to a stronger wake, as compared to LBM. These observations highlight the criticality of selecting an appropriate fidelity level, especially when complex 3D fluid dynamic interactions are present in a rotor setup, and an opportunity for improvement in the predictions by the mid-fidelity method.

The investigation also compares the aeroacoustic properties across the three VAWT configurations, using only the high-fidelity LBM. It is noted that the inclusion of struts and tower results in a decline in low-frequency noise, correlating with the observed reduction in integral blade loading or thrust. In contrast, high-frequency noise increases due to higher intensity of interactions between the blade and wake vortices shedding from upstream structures.

Future studies should explore the change in optimal TSR value with additional support structures, keeping VAWT blade design and solidity constant (to allow changes in force and flow field only due to the support structures and not any other VAWT design parameter). The airfoil polar data within the LLFVW framework can be refined and empirical modifications be made to more accurately reflect blade-wake and blade-vortex interactions, also aligning with experimental results. Furthermore, due to the large 3D design space of VAWTs, there is a need for high-fidelity investigation into the effect of other geometric parameters, such as the effect of the airfoil shape, aspect ratio, blade design and blade pitch, as well as flow parameters, such as non-uniform inflow, on both aerodynamic performance and noise generation. An extension of the current study will explore such topics along with real-life experimental results to be obtained from a helical-bladed small-scale VAWT installed at Nottingham Trent University, UK.



## Acknowledgments

This project has received funding from the European Union's Horizon 2020 Marie Curie zEPHYR research and innovation programme under grant agreement No EC grant 860101 (https://www.h2020-zephyr.eu/). Nottingham Trent University has received sponsorship from 3DS Simulia for the commercial software PowerFLOW. Special thanks to a few researchers for a thoughtful discussion on the PowerFLOW simulations - Gianluca Romani and Edoardo Grande, and on the QBlade simulations - Adhyanth Giri Ajay and David Marten; and thanks to Damiano Casalino for sharing with me his *optydb* tool.

## References

[1] Europe, W., "Wind energy in Europe: 2022 Statistics and the outlook for 2023-2027," *Brussels, Belgium. Available online at: https://windeurope.org/intelligence-platform/product/wind-energy-in-europe-2022-statistics-and-the-outlook-for-2023-2027/*, 2023.

[2] Micallef, D., and Van Bussel, G., "A review of urban wind energy research: aerodynamics and other challenges," *Energies*, Vol. 11, No. 9, 2018, p. 2204.

[3] Kumar, R., Raahemifar, K., and Fung, A. S., "A critical review of vertical axis wind turbines for urban applications," *Renewable and Sustainable Energy Reviews*, Vol. 89, 2018, pp. 281–291.

[4] Peng, H., Liu, H., and Yang, J., "A review on the wake aerodynamics of H-rotor vertical axis wind turbines," *energy*, Vol. 232, 2021, p. 121003.

[5] Du, L., Ingram, G., and Dominy, R. G., "A review of H-Darrieus wind turbine aerodynamic research," *Proceedings of the Institution of Mechanical Engineers, Part C: Journal of Mechanical Engineering Science*, Vol. 233, No. 23-24, 2019, pp. 7590–7616.

[6] Sutherland, H. J., Berg, D. E., and Ashwill, T. D., "A retrospective of VAWT technology," *Sandia National Laboratories*, 2012, pp. 1–64.

[7] Marie, D. G. J., "Turbine having its rotating shaft transverse to the flow of the current," , Dec. 8 1931. US Patent 1,835,018.

[8] Wilson, R. E., and Lissaman, P. B., "Applied aerodynamics of wind power machines," *National Science Foundation*, 1974.

[9] Le Gourieres, D., *Wind power plants: theory and design*, Elsevier, 2014.

[10] Shubham, S., Naik, K., Sachar, S., and Ianakiev, A., "Performance analysis of low Reynolds number vertical axis wind turbines using low-fidelity and mid-fidelity methods and wind conditions in the city of Nottingham," *Energy*, Vol. 279, 2023, p. 127904.

[11] Howell, R., Qin, N., Edwards, J., and Durrani, N., "Wind tunnel and numerical study of a small vertical axis wind turbine," *Renewable energy*, Vol. 35, No. 2, 2010, pp. 412–422.

[12] Cheng, Q., Liu, X., Ji, H. S., Kim, K. C., and Yang, B., "Aerodynamic analysis of a helical vertical axis wind turbine," *Energies*, Vol. 10, No. 4, 2017, p. 575.

[13] Lam, H., and Peng, H., "Study of wake characteristics of a vertical axis wind turbine by two-and three-dimensional computational fluid dynamics simulations," *Renewable Energy*, Vol. 90, 2016, pp. 386–398.

[14] Li, C., Zhu, S., Xu, Y.-l., and Xiao, Y., "2.5 D large eddy simulation of vertical axis wind turbine in consideration of high angle of attack flow," *Renewable energy*, Vol. 51, 2013, pp. 317–330.

[15] Zhang, L., Liang, Y., Liu, X., Jiao, Q., and Guo, J., "Aerodynamic performance prediction of straight-bladed vertical axis wind turbine based on CFD," *Advances in Mechanical Engineering*, Vol. 5, 2013, p. 905379.

[16] Elkhoury, M., Kiwata, T., and Aoun, E., "Experimental and numerical investigation of a three-dimensional vertical-axis wind turbine with variable-pitch," *Journal of wind engineering and Industrial aerodynamics*, Vol. 139, 2015, pp. 111–123.

[17] Miao, W., Liu, Q., Zhang, Q., Xu, Z., Li, C., Yue, M., Zhang, W., and Ye, Z., "Recommendation for strut designs of vertical axis wind turbines: Effects of strut profiles and connecting configurations on the aerodynamic performance," *Energy Conversion and Management*, Vol. 276, 2023, p. 116436.

[18] Siddiqui, M. S., Durrani, N., and Akhtar, I., "Numerical study to quantify the effects of struts and central hub on the performance of a three dimensional vertical axis wind turbine using sliding mesh," *ASME Power Conference*, Vol. 56062, American Society of Mechanical Engineers, 2013, p. V002T09A020.

[19] De Marco, A., Coiro, D. P., Cucco, D., and Nicolosi, F., "A numerical study on a vertical-axis wind turbine with inclined arms," *International Journal of Aerospace Engineering*, Vol. 2014, 2014.

[20] Shubham, S., Ianakiev, A., and Wright, N., "Review of standalone small-scale Darrieus wind turbines - a Nottingham case study," *17th EAWE PhD Seminar on Wind Energy*, 2021.

[21] Aihara, A., Mendoza, V., Goude, A., and Bernhoff, H., "A numerical study of strut and tower influence on the performance of vertical axis wind turbines using computational fluid dynamics simulation," *Wind Energy*, Vol. 25, No. 5, 2022, pp. 897–913.

[22] Bachant, P., Wosnik, M., Gunawan, B., and Neary, V. S., "Experimental study of a reference model vertical-axis cross-flow turbine," *PloS one*, Vol. 11, No. 9, 2016, p. e0163799.

[23] Hara, Y., Jodai, Y., Yamamoto, S., and Okinaga, T., "Numerical Simulation on Tandem Layout of Two Vertical Axis Wind Turbines," *Proceedings of the 2019 Annual General Meeting, JSME, Akita, Japan*, Vol. 10, 2019.

[24] Ahmadi-Baloutaki, M., Carriveau, R., and Ting, D. S., "Straight-bladed vertical axis wind turbine rotor design guide based on aerodynamic performance and loading analysis," *Proceedings of the Institution of Mechanical Engineers, Part A: Journal of Power and Energy*, Vol. 228, No. 7, 2014, pp. 742–759.

[25] Lu, W., "Aerodynamic modelling of vertical axis wind turbine struts: Using the lifting line method CACTUS," 2020.

[26] Mendoza, V., Bachant, P., Ferreira, C., and Goude, A., "Near-wake flow simulation of a vertical axis turbine using an actuator line model," *Wind Energy*, Vol. 22, No. 2, 2019, pp. 171–188.

[27] Bakker, R. H., Pedersen, E., van den Berg, G. P., Stewart, R. E., Lok, W., and Bouma, J., "Impact of wind turbine sound on annoyance, self-reported sleep disturbance and psychological distress," *Science of the total environment*, Vol. 425, 2012, pp. 42–51.

[28] Klæboe, R., and Sundfør, H. B., "Windmill noise annoyance, visual aesthetics, and attitudes towards renewable energy sources," *International journal of environmental research and public health*, Vol. 13, No. 8, 2016, p. 746.

[29] Möllerström, E., Ottermo, F., Hylander, J., and Bernhoff, H., "Noise emission of a 200 kW vertical axis wind turbine," *Energies*, Vol. 9, No. 1, 2016, p. 19.

[30] Möllerström, E., Larsson, S., Ottermo, F., Hylander, J., and Bååth, L., "Noise propagation from a vertical axis wind turbine," *inter. noise 2014, 43rd International Congress on Noise Control Engineering, Melbourne, Australia, November 16-19, 2014*, Australian Acoustical Society, 2014.

[31] Dumitrescu, H., Cardos, V., Dumitrache, A., and Frunzulica, F., "Low-frequency noise prediction of vertical axis wind turbines," *Proceedings of the Romanian Academy*, Vol. 11, No. 1, 2010, pp. 47–54.

[32] Shubham, S., Wright, N., Avallone, F., and Ianakiev, A., "Aerodynamic and aeroacoustic investigation of vertical axis wind turbines with different number of blades using mid-fidelity and high-fidelity methods," *AIAA AVIATION 2023 Forum*, 2023, p. 3642.

[33] Ramprakash, T. T., Shubham, S., and Ianakiev, A., "Effect of Blade Shape on Aerodynamic and Aeroacoustic characteristics of Vertical Axis Wind Turbines using mid-fidelity and high-fidelity methods," *AIAA SciTech Forum*, 2024.

[34] Shubham, S., Kipouros, T., Dash, S., and Ianakiev, A., "Uncertainty propagation and management of mixed uncertainties for multi-fidelity multi-disciplinary analysis of propeller with different blade sweep," *AIAA SciTech Forum*, 2024.

[35] Marten, D., Bianchini, A., Pechlivanoglou, G., Balduzzi, F., Nayeri, C. N., Ferrara, G., Paschereit, C. O., and Ferrari, L., "Effects of airfoil's polar data in the stall region on the estimation of Darrieus wind turbine performance," *Journal of Engineering for Gas Turbines and Power*, Vol. 139, No. 2, 2017.

[36] Balduzzi, F., Marten, D., Bianchini, A., Drofelnik, J., Ferrari, L., Campobasso, M. S., Pechlivanoglou, G., Nayeri, C. N., Ferrara, G., and Paschereit, C. O., "Three-dimensional aerodynamic analysis of a Darrieus wind turbine blade using computational fluid dynamics and lifting line theory," *Journal of Engineering for Gas Turbines and Power*, Vol. 140, No. 2, 2018.

[37] Van Garrel, A., "Development of a wind turbine aerodynamics simulation module," 2003.

[38] Marten, D., "QBlade Guidelines v0. 95," *Technical University of Berlin, Berlin, Germany*, 2016.

[39] Marten, D., Lennie, M., Pechlivanoglou, G., Nayeri, C. N., and Paschereit, C. O., "Implementation, optimization, and validation of a nonlinear lifting line-free vortex wake module within the wind turbine simulation code qblade," *Journal of Engineering for Gas Turbines and Power*, Vol. 138, No. 7, 2016.

[40] Marten, D., Pechlivanoglou, G., Navid Nayeri, C., and Oliver Paschereit, C., "Nonlinear lifting line theory applied to vertical axis wind turbines: Development of a practical design tool," *Journal of Fluids Engineering*, Vol. 140, No. 2, 2018.

[41] Bergami, L., and Gaunaa, M., "ATEFlap Aerodynamic Model, a dynamic stall model including the effects of trailing edge flap deflection," 2012.

[42] Wendler, J., Marten, D., Pechlivanoglou, G., Nayeri, C. N., and Paschereit, C. O., "An unsteady aerodynamics model for lifting line free vortex wake simulations of hawt and vawt in qblade," *Turbo Expo: Power for Land, Sea, and Air*, Vol. 49873, American Society of Mechanical Engineers, 2016, p. V009T46A011.

[43] Brandetti, L., Avallone, F., De Tavernier, D., LeBlanc, B., Ferreira, C. S., and Casalino, D., "Assessment through high-fidelity simulations of a low-fidelity noise prediction tool for a vertical-axis wind turbine," *Journal of Sound and Vibration*, Vol. 547, 2023, p. 117486.

[44] Gourdain, N., Jardin, T., Serre, R., Prothin, S., and Moschetta, J.-M., "Application of a lattice Boltzmann method to some challenges related to micro-air vehicles," *International Journal of Micro Air Vehicles*, Vol. 10, No. 3, 2018, pp. 285–299.

[45] Shubham, S., Avallone, F., Grande, E., and Casalino, D., "Computational Aeroacoustic Investigation of Co-rotating rotors for Urban Air Mobility," *Delft International Conference on Urban Air-Mobility*, 2021.

[46] Shubham, S., "Computational Aeroacoustic Investigation of Co-rotating rotors for Urban Air Mobility," 2020.

[47] Avallone, F., van den Ende, L., Li, Q., Ragni, D., Casalino, D., Eitelberg, G., and Veldhuis, L., "Aerodynamic and aeroacoustic effects of swirl recovery vanes length," *Journal of Aircraft*, Vol. 56, No. 6, 2019, pp. 2223–2235.

[48] Casalino, D., Hazir, A., and Mann, A., "Turbofan broadband noise prediction using the lattice Boltzmann method," *AIAA Journal*, Vol. 56, No. 2, 2018, pp. 609–628.

[49] Nardari, C., Casalino, D., Polidoro, F., Coralic, V., Lew, P.-T., and Brodie, J., "Numerical and experimental investigation of flow confinement effects on UAV rotor noise," *25th AIAA/CEAS Aeroacoustics Conference*, 2019, p. 2497.

[50] Succi, S., *The lattice Boltzmann equation for fluid dynamics and beyond*, 1st ed., Clarendon Press, Oxford, 2001.

[51] Shan, X., Yuan, X.-F., and Chen, H., "Kinetic theory representation of hydrodynamics: a way beyond the Navier–Stokes equation," *Journal of Fluid Mechanics*, Vol. 550, 2006, pp. 413–441. https://doi.org/10.1017/S0022112005008153, URL http://www.journals.cambridge.org/abstract_S0022112005008153.

[52] Chen, S., and Doolen, G., "Lattice Boltzmann method for fluid flows," *Annual Review of Fluid Mechanics*, Vol. 30, No. 1, 1998, pp. 329–364. https://doi.org/10.1146/annurev.fluid.30.1.329, URL http://www.annualreviews.org/doi/10.1146/annurev.fluid.30.1.329.

[53] Chen, H., Chen, S., and Matthaeus, W., "Recovery of the Navier-Stokes equations using a lattice-gas Boltzmann method," *Physical Review A*, Vol. 45, No. 8, 1992, pp. R5339–R5342. https://doi.org/10.1103/PhysRevA.45.R5339, URL https://link.aps.org/doi/10.1103/PhysRevA.45.R5339.

[54] Chen, H., Zhang, R., and Gopalakrishnan, P., "Lattice Boltzmann Collision Operators Enforcing Isotropy and Galilean Invariance," , 8 2015. URL https://patents.google.com/patent/US20150356217A1/en.

[55] Yakhot, V., and Orszag, S., "Renormalization group analysis of turbulence. I. Basic theory," *Journal of Scientific Computing*, Vol. 1, No. 1, 1986, pp. 3–51. https://doi.org/10.1007/BF01061452, URL http://link.springer.com/10.1007/BF01061452.

[56] Teixeira, C., "Incorporating Turbulence Models into the Lattice-Boltzmann Method," *International Journal of Modern Physics C*, Vol. 09, No. 08, 1998, pp. 1159–1175. https://doi.org/10.1142/S0129183198001060, URL http://www.worldscientific.com/doi/abs/10.1142/S0129183198001060.

[57] Wilcox, D., *Turbulence modelling for CFD (Third Edition)*, DCW Industries, Incorporated, 2006.

[58] Launder, B., and Spalding, D., "The numerical computation of turbulent flows," *Computer Methods in Applied Mechanics and Engineering*, Vol. 3, No. 2, 1974, pp. 269–289. https://doi.org/10.1016/0045-7825(74)90029-2, URL http://www.sciencedirect.com/science/article/pii/0045782574900292.

[59] Ffowcs Williams, J. E., and Hawkings, D. L., "Sound generation by turbulence and surfaces in arbitrary motion," *Philosophical Transactions of the Royal Society of London. Series A, Mathematical and Physical Sciences*, Vol. 264, No. 1151, 1969, pp. 321–342.

[60] Farassat, F., and Succi, G. P., "A review of propeller discrete frequency noise prediction technology with emphasis on two current methods for time domain calculations," *Journal of Sound and Vibration*, Vol. 71, No. 3, 1980, pp. 399–419.

[61] Brès, G., Pérot, F., and Freed, D., "Properties of the lattice Boltzmann method for acoustics," *15th AIAA/CEAS Aeroacoustics Conference (30th AIAA Aeroacoustics Conference)*, 2009, p. 3395.

[62] Casalino, D., "An advanced time approach for acoustic analogy predictions," *Journal of Sound and Vibration*, Vol. 261, No. 4, 2003, pp. 583–612.

[63] LeBlanc, B., and Simao Ferreira, C., "Overview and design of pitchvawt: Vertical axis wind turbine with active variable pitch for experimental and numerical comparison," *2018 Wind Energy Symposium*, 2018, p. 1243.

[64] LeBlanc, B., and Ferreira, C., "Estimation of blade loads for a variable pitch vertical axis wind turbine from particle image velocimetry," *Wind Energy*, Vol. 25, No. 2, 2022, pp. 313–332.

[65] Drela, M., "XFOIL: An analysis and design system for low Reynolds number airfoils," *Low Reynolds number aerodynamics*, Springer, 1989, pp. 1–12.

[66] Montgomerie, B., "Methods for root effects, tip effects and extending the angle of attack range to±180, with application to aerodynamics for blades on wind turbines and propellers," *FOI, Swedish Defence Research Agency, Stockholm, Sweden, Report No. FOI*, 2004.

[67] Holst, K. R., Glasby, R. S., and Bond, R. B., "On the effect of temporal error in high-order simulations of unsteady flows," *Journal of Computational Physics*, Vol. 402, 2020, p. 108989.

[68] Shubham, S., Wright, N., and Ianakiev, A., "Application of Richardson extrapolation method to aerodynamic and aeroacoustic characteristics of low Reynolds number vertical axis wind turbines," *28th AIAA/CEAS Aeroacoustics 2022 Conference*, 2022, p. 3022.

[69] Rezaeiha, A., Kalkman, I., and Blocken, B., "CFD simulation of a vertical axis wind turbine operating at a moderate tip speed ratio: Guidelines for minimum domain size and azimuthal increment," *Renewable energy*, Vol. 107, 2017, pp. 373–385.

[70] Meana-Fernández, A., Fernandez Oro, J. M., Argüelles Díaz, K. M., Galdo-Vega, M., and Velarde-Suárez, S., "Application of Richardson extrapolation method to the CFD simulation of vertical-axis wind turbines and analysis of the flow field," *Engineering Applications of Computational Fluid Mechanics*, Vol. 13, No. 1, 2019, pp. 359–376.

[71] Vassberg, J., "Challenges and accomplishments of the AIAA CFD drag prediction workshop series," *AVT-246 Specialists' Meeting on Progress and Challenges in Validation Testing for Computational Fluid Dynamics, Avila, Spain, Sept*, 2016, pp. 26–28.

[72] Glegg, S., and Devenport, W., *Aeroacoustics of low Mach number flows: fundamentals, analysis, and measurement*, Academic Press, 2017.

[73] Pearson, C., "Vertical axis wind turbine acoustics," Ph.D. thesis, University of Cambridge, 2014.

[74] Weber, J., Riedel, S., Praß, J., Renz, A., Becker, S., and Franke, J., "Effect of Boundary Layer Tripping on the Aeroacoustics of Small Vertical Axis Wind Turbines," *Advanced Engineering Forum*, Vol. 19, Trans Tech Publ, 2016, pp. 3–9.

[75] De Oliveira, G., Pereira, R., Timmer, N., and Van Rooij, R., "Improved airfoil polar predictions with data-driven boundary-layer closure relations," *Journal of Physics: Conference Series*, Vol. 1037, IOP Publishing, 2018, p. 022009.

[76] Sheldahl, R. E., and Klimas, P. C., "Aerodynamic characteristics of seven symmetrical airfoil sections through 180-degree angle of attack for use in aerodynamic analysis of vertical axis wind turbines," Tech. rep., Sandia National Labs., Albuquerque, NM (USA), 1981.

[77] Imiela, M., Faßmann, B., Heilers, G., and Wilke, G., "Numerical airfoil catalogue including 360 airfoil polars and aeroacoustic footprints," *Wind Energy Science Discussions*, 2017, pp. 1–34.

[78] Avallone, F., Ragni, D., and Casalino, D., "On the effect of the tip-clearance ratio on the aeroacoustics of a diffuser-augmented wind turbine," *Renewable Energy*, Vol. 152, 2020, pp. 1317–1327.

[79] Lignarolo, L., Ragni, D., Scarano, F., Ferreira, C. S., and Van Bussel, G., "Tip-vortex instability and turbulent mixing in wind-turbine wakes," *Journal of Fluid Mechanics*, Vol. 781, 2015, pp. 467–493.